Wind turbine optimization

Yesitai Keleshibieke, B.Eng

Submitted in fulfillment of the requirements
For the degree of Masters of Science
in Mechanical Engineering

School of Engineering
Department of Mechanical Engineering
Nazarbayev University

53 Kabanbay Batyr Avenue,
Astana,Kazakhstan,010000

Supervisors: Yong Zhao,Soo Lee The,Sai Fok
2018.12.10

Abstract

Facing the current extreme global environmental and energy crisis, wind energy, as a source of renewable energy, is becoming more and more crucial to the future development of human civilization. Wind energy technology is already well developed and widely used around the world. Currently, horizontal axis wind turbines (HAWT) are the most common and efficient type of wind turbines that are widely used in commercial wind farms. And the key to greater power output and high efficiency lies in the design of wind turbine blades. Thus, the design optimization of wind turbine blades plays a significant role in achieving our goal.

In this thesis, the current research status, design theory, and methods are reviewed; and blade efficiency, torques and force coefficients of wind turbine blades are analyzed. This study is based on the momentum-blade element theory and CFD method. The NREL Phase VI blade model is built. A truly 3D optimization platform, consisting of Solidworks, Ansys Fluent and Ansys Workbench/Design Xplorer, is used in the optimization process, in which a direct optimization method is adopted for the aerodynamic optimization of the NREL Phase VI turbine blade. The average power output of the turbine is set as a goal of optimization which should be maximized during the optimization process. To achieve that, the positions of the trailing edges on 20 cross sections are set as independent variables which change within a certain range to achieve maximum power output. As a result, the power output increases by over 9 percent and proves the accuracy and feasibility of the optimization methodology.

Keywords: wind turbine optimization, numerical simulation, CFD, BEM, IBEM, genetic algorithm, GDO.

Content

1.Background:....8
1.1.Development and Theories of Wind Turbine Design....9
1.1.1 Historical Development of Wind Turbines....9
1.1.2 Wind Power Potential in Kazakhstan....13
2. Literatur Review....16
2.1 Different Types of Wind Turbines....18
2.2 Design and Construction of Wind Turbines....21
2.3 Basic Theories and Methods of Wind Turbine Design Optimization....23
2.4 Latest Work in Wind Turbine Design Optimization....23
2.5 Goal and Scope of Research....26
3. Fundamental Theories....27
3.1 Basic Theories....27
3.1.1 Momentum Theory and Betz's Limit....27
3.1.2 Blade Element Theory....30
3.1.3 Blade Element Momentum Theory....31
4. CFD Analysis and Optimization of Wind Turbine Blades....32
4.1 Inverse Blade Element Momentum Theory (IBEM)....32
4.2 CFD study of NREL PHASE VI Rotor....32
4.2.1 Governing Equations....33
4.2.2 Numerical Methods and Boundary Conditions
4..2.3 Mesh Convergence Study and Validation of CFD Model
4.2.3.1 Mesh Convergence Study
4.2.3.1 Validation of CFD Results and Model
4.3 Optimization Method: Goal Driven Optimization(GDO)....46
5.Final optimization results:....56
6.Conclusion:....63

List of Abbreviation

CFD – Computational Fluid Dynamics
NS – Navier-Stokes
RANS - Reynolds-averaged Navier–Stokes
IBEM – Inverse Blade Element Momentum
BEM – Blade Element Momentum
CAD – Computer Aided Design
NREL – National Renewable Energy Laboratory
FEM – Finite Element Method

MRF - Moving Reference Frame
GDO – Goal Driven Optimization
Screening – Shifted Hammersley
MOGA – Multi-objective Genetic Algorithm),
NLPQL – Non-linear Programming by Quadratic Lagrangian
MISQP – Mixed-Integer Sequential Quadratic Programming

List of Tables

Table 1: Input design parameter set……...50
Table 2: Output: ranges of optimized design parameter set……..51
Table 3: Discrete input parameters in parameter set……...52
Table 4: geometric parameter of 3 blade models…….....55
Table 5: CFD simulation results of 3 models…….55
Table 6: Computation requirements...……... …….56
Table 7: Optimal design points and power output…….56
Table 8: Comparison with the original model…… 57

List of Figures

Figure 1: Global wind capacity……..11
Figure 2: TOP 10 cumulative capacity……...11
Figure 3: Global wind capacity……..12
Figure 4: Solar energy distribution……13
Figure5: Wind energy distribution ……...13
Figure 6: Hydro potential distribution……...14
Figure 7: Geothermal energy in Kazakhstan…….15
Figure 8: Annual wind speed distribution in Kazakhstan…….15
Figure 9: Oriol Lehmkuhl-simplified methods for wind turbine blade design…….17
Figure 10: Lift and drag coefficient vs angle of attack…….17
Figure 11: stall development…….18
Figure 12: Control volume……28
Figure 13: Forces and velocities for a blade element……31
Figure 14: S809 foil shape of NREL phase VI wind turbine……..37
Figure 15: Simulation geometry in ANSYS FLUENT……..37
Figure 16: Rotating domain……...38
Figure 17: Mesh around blade surface……...38
Figure 18: CFD calculation residuals……39
Figure 19: results of mesh refinement study……..40
Figure 20: pressure coefficient at 30 percent span……41
Figure 21: pressure coefficient at 47 percent span……41
Figure 22: pressure coefficient at 63 percent span……42
Figure 23: pressure coefficient at 80 percent span……42
Figure 24: pressure coefficient at 95 percent span……43
Figure 25: wall Y plus contour……..43
Figure 26: NREL NASA experiment turbine components……44
Figure 27: Simplified foil shape and design parameter……..47
Figure 28: blade model……..47
Figure 29: Direct Optimization Structure……..48
Figure 30:NLPQL optimization process……50
Figure 31:MISQP optimization

process…….54
Figure 32: Pressure contour at 47 percent span…….58
Figure 33: Pressure contour at 63 percent span…….59
Figure 34: Pressure contour at 80 percent span…….60
Figure 35: Pressure contour at 95 percent span…….61

1.Background:

According to a report from the International Energy Agency, the reserves of coal, natural gas, and oil can last 200.50 and 30 years respectively. All three energy resources**[1]** can be categorized as fossil fuel that cannot be regenerated and recycled. Thus the development of alternatives for future energy is of great significance and urgency. It is assumed that nuclear power, solar power, wind power, hydropower, geothermal power will be the main power resource in the 21 century.

The modern economy relies heavily on the consumption of energy, especially fossil fuel. Along with the economic growth and population growth, the demand for energy increases fast, so is the greenhouse gas emission that caused climate change which now affects the environment severely especially in coastal areas. However, it is a cruel fact that we are running out of fossil fuel and the promise to cut carbon emission did not make promising progress and commercial and industrial activity heavily depend on energy. To ensure economic development, mankind has managed to generate power from natural resources, wind power is one of the alternatives of renewable energy. The utilization of wind power can be traced back to 3000 years ago when wind power is used to drive boats and windmills to make flour. However, the utilization of wind power to generate electricity can only be traced back to 19th century and the generators during that period can only generate a small amount of electricity that is only enough to charge batteries and is not stable and sustainable. Through decades of development and industrial application, the technology of wind turbine seems mature enough. Nevertheless, a wind tunnel experiment carried out by an institution in China and the report shows that current horizontal axis wind turbine can only reach an efficiency with a range from 23%-29% **[2]**, which means there is still a space for improvement considering the theoretical maximum by Betz limit is 59.3%. In addition, a growing number of small wind turbines are been used to generate power for traffic lights and road lights in some less populated areas and highways. Moreover, some small wind turbines have a capacity sufficient to supply the daily power consumption of a family in suburban and rural areas, which significantly reduces the energy loss in transmission.

With the development of wind power technology, a growing number of wind farms have been installed across the world even offshore or in mountainous areas and wind power has become sustainable and reliable clean and renewable power resource. Take all into consideration, we can come to the conclusion that wind power will be a major energy alternative in the post-fossil fuel era.

1.1.Development and theories of Wind Turbine Design

1.1.1 Historical Development of Wind Turbines

Mankind has a long history manipulating wind to achieve a certain goal. However, the temptation of wind power generation began in Denmark in the late

19th century. The stimulus for wind energy development is the oil crisis in 1973. After the crisis, America and other developed countries realized the urgency of developing sustainable and renewable energy as an alternative to oil and gas. Thus, tons of money and time was spent on the development of renewable energy. With the development and breakthrough of computer science and theories of aerodynamics, structural mechanics, and new materials, huge progress is made to utilize wind power. During that period, engineers in those government-funded programs tried several different types of architecture and the concept of 'Danish' **[3]** wind turbine, a horizontal axis wind turbine with 3 blades,stall-regulated rotor, and a fixed-speed, induction machine drive train, emerged. The concept is later proved most efficient and implemented in industrial wind turbine designing. Since then new concepts emerged such as controlled blades and variable-speed operation. And the power output capacity of the single industrial power generating wind turbine grew from 55KW, in the 80s, to 4 MW in 90s, which reduced the price of wind-generated electricity to 5 cents per kWh and made it possible to compete with the conventional power plant. At the same time, the annual utilization rate rose from 60% to over 95% **[4]**. The wind power becomes increasingly reliable and compatible as a result of achievements through decades of innovation and hard work of engineers.

A report from Global Wind Energy Council(GWEC) shows that in 2016, there was over 54 GW of renewable clean wind power installed across the world comprising over 90 countries. 9 of them have installed more than 10000MW as well as 29 countries that have passed the mark of 1000MW. The total capacity reached 486.8GW with an annual growth of 12.6%. And GWEC indicates that the global wind power capacity will reach 800 GW by 2021**[5,18]**.

As we can see, the wind power is becoming a main player in the global energy market and successfully competing with dominant incumbents like polluting plants, which is also a huge step forward towards a clean future.

Figure 1: Global wind capacity

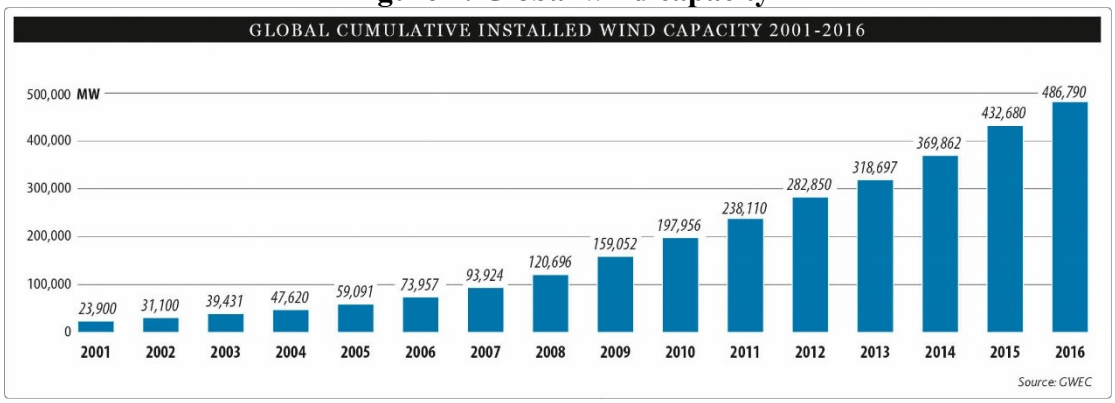

Figure 2: TOP 10 cumulative capacity

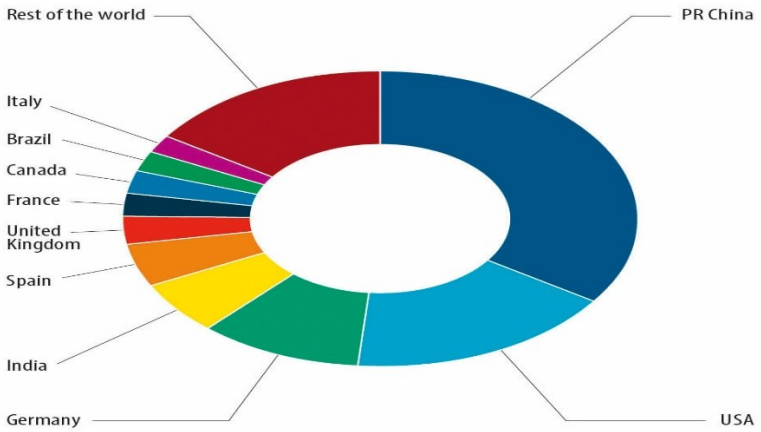

Country	MW	% Share
PR China	168,732	34.7
USA	82,184	16.9
Germany	50,018	10.3
India	28,700	5.9
Spain	23,074	4.7
United Kingdom	14,543	3.0
France	12,066	2.5
Canada	11,900	2.4
Brazil*	10,740	2.2
Italy	9,257	1.9
Rest of the world	75,576	15.5
Total TOP 10	**411,214**	**84**
World Total	**486,790**	**100**

As the global warming effects get increasingly severe, the desire to cut carbon emission becomes stronger. The only way to achieve that goal and ensure the global economic growth is to develop clean renewable energy, which can also create hundreds of thousands of jobs. In spite of solar and hydropower, wind power is becoming a reliable energy resource. Whatsmore, with the development of technology and material science, the unit capacity grows which means fewer units are needed to generate the same amount of power and also more power can be generated in the same wind field.

Figure 3: Global wind capacity

GLOBAL INSTALLED WIND POWER CAPACITY (MW) – REGIONAL DISTRIBUTION

		End 2015	New 2016	Total 2016
AFRICA & MIDDLE EAST				
	South Africa	1,053	418	1,471
	Egypt	810	-	810
	Morocco	787	-	787
	Ethiopia	324	-	324
	Tunisia	245	-	245
	Jordan	119	-	119
	Other[1]	150	-	150
	Total	**3,488**	**418**	**3,906**
ASIA				
	PR China	145,362	23,370	168,732
	India	25,088	3,612	28,700
	Japan	3,038	196	3,234
	South Korea	835	201	1,031
	Taiwan	647	35	682
	Pakistan	308	282	591
	Thailand	223	-	223
	Philippines	216	-	216
	Other[2]	253	25	276
	Total	**175,970**	**27,721**	**203,685**
EUROPE				
	Germany	44,941	5,443	50,018
	Spain	23,025	49	23,074
	UK	13,809	736	14,543
	France	10,505	1,561	12,066
	Italy	8,975	282	9,257
	Sweden	6,029	493	6,520
	Turkey	4,694	1,387	6,081
	Poland	5,100	682	5,782
	Portugal	5,050	268	5,316
	Denmark	5,064	220	5,228
	Netherlands	3,443	887	4,328
	Romania	2,976	52	3,028
	Ireland	2,446	384	2,830
	Austria	2,404	228	2,632
	Belgium	2,218	177	2,386
	Rest of Europe[3]	7,220	1,077	8,241
	Total Europe	**147,899**	**13,926**	**161,330**
	of which EU-28[4]	141,721	12,491	153,729
LATIN AMERICA & CARIBBEAN				
	Brazil*	8,726	2,014	10,740
	Chile	911	513	1,424
	Uruguay	845	365	1,210
	Argentina	279	-	279
	Costa Rica	278	20	298
	Panama	270	-	270
	Peru	148	93	241
	Honduras	176	-	176
	Dominican Republic	86	50	135
	Caribbean[5]	164	-	164
	Others[6]	335	24	359
	Total	**12,218**	**3,079**	**15,296**
NORTH AMERICA				
	USA	73,991	8,203	82,184
	Canada	11,219	702	11,900
	Mexico	3,073	454	3,527
	Total	**88,283**	**9,359**	**97,611**
PACIFIC REGION				
	Australia	4,187	140	4,327
	New Zealand	623	-	623
	Pacific Islands	13	-	13
	Total	**4,823**	**140**	**4,963**
	World total	**432,680**	**54,642**	**486,790**

Source: GWEC

1 Algeria, Cape Verde, Iran, Israel, Kenya, Libya, Nigeria
2 Bangladesh, Mongolia, Sri Lanka, Vietnam
3 Bulgaria, Cyprus, Czech Republic, Estonia, Finland, Faroe Islands, FYROM, Hungary, Iceland, Latvia, Liechtenstein, Lithuania, Luxembourg, Malta, Norway, Romania, Russia, Switzerland, Slovakia, Slovenia, Ukraine
4 Austria, Belgium, Bulgaria, Cyprus, Croatia, Czech Republic, Denmark, Estonia, Finland, France, Germany, Greece, Hungary, Ireland, Italy, Latvia, Lithuania, Luxembourg, Malta, Netherlands, Poland, Portugal, Romania, Slovakia, Slovenia, Spain, Sweden, UK
5 Caribbean: Aruba, Bonaire, Curacao, Cuba, Dominica, Guadalupe, Jamaica, Martinica, Granada, St. Kitts and Nevis
6 Bolivia, Colombia, Ecuador, Guatemala, Nicaragua, Venezuela

Note: Project decommissioning of approximately 520 MW and rounding affect the final sums
** Projects fully commissioned, grid connections pending in some cases*

1.1.2 Wind Power Potential in Kazakhstan

Speaking of Kazakhstan, as a main oil exporter in the global oil market, Kazakhstan also has a considerable potential to produce clean and renewable energy.

Figure 4: Solar energy distribution

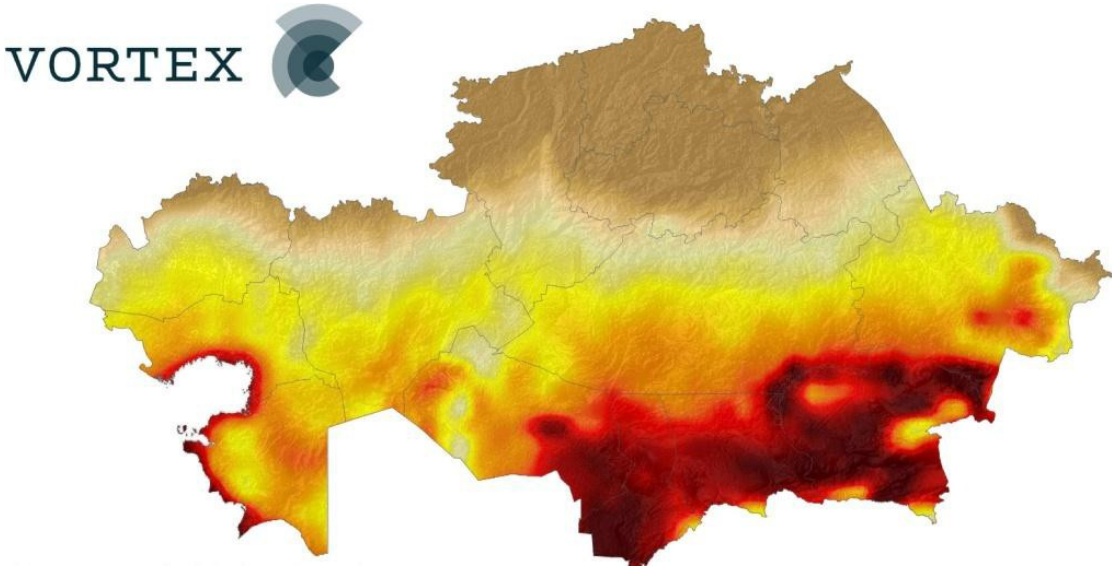

According to a recent report by KAZENERGY, the total potential of solar energy nationwide can reach 3700000TWh theoretically**[6]**.

Figure 5: Wind energy distribution

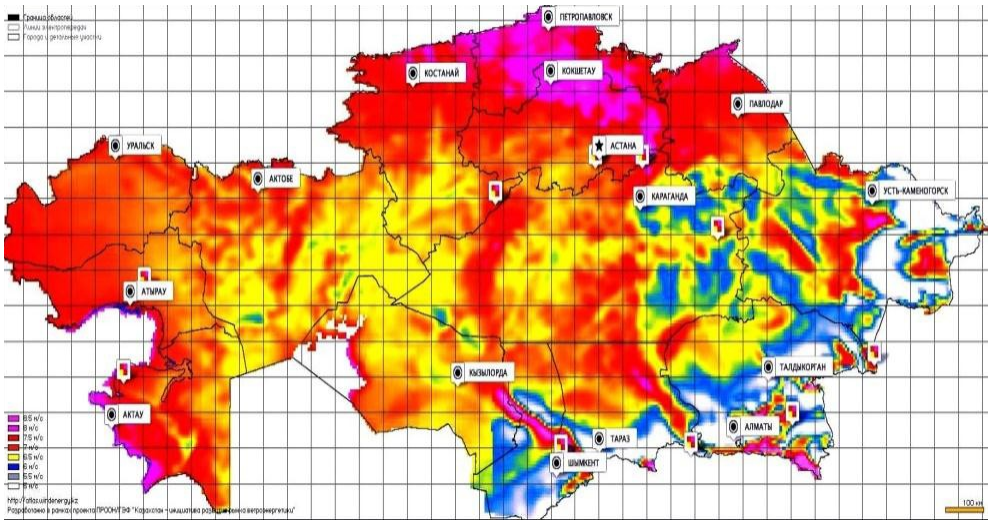

Where wind power potential ranks second with a theoretically approximated amount of 14098TWh. As is shown in the graph above, most of the northern part of Kazakhstan is rich in wind resource. Considering the small population and the low population density, most of the rural region of northern and central west Kazakhstan is ideal to be a windmill field.

On the contrary, Kazakhstan, as a landlocked country with few rivers and a low precipitation rate, only has a low hydro potential as is given in the report with an amount of 170TWh and is concentrated mainly in the eastern region of Kazakhstan. And in terms of geothermal energy, the potential is approximated as 38 TWh.

Figure 6: Hydro potential distribution

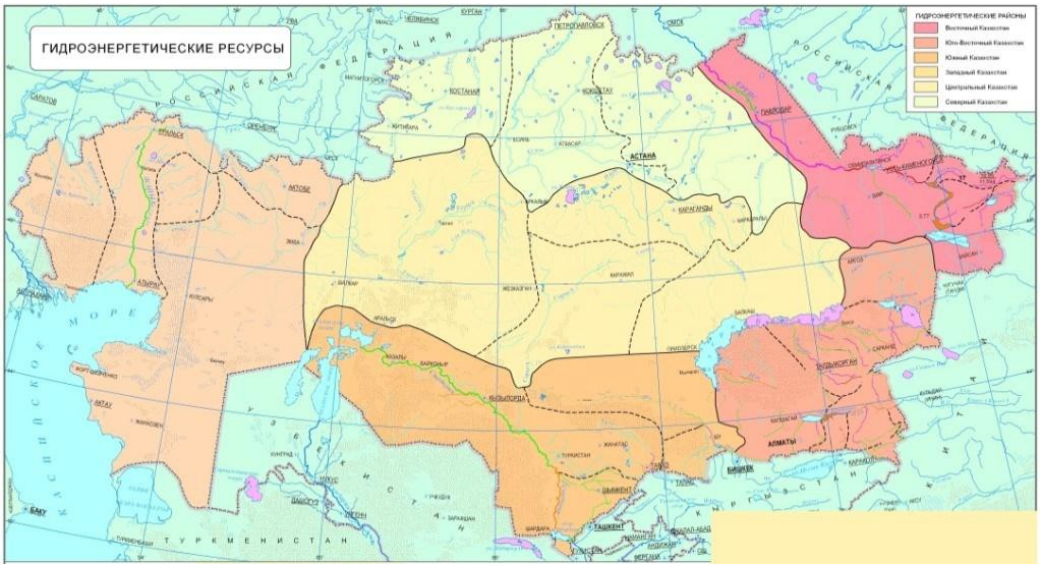

Figure 7: Geothermal energy in Kazakhstan

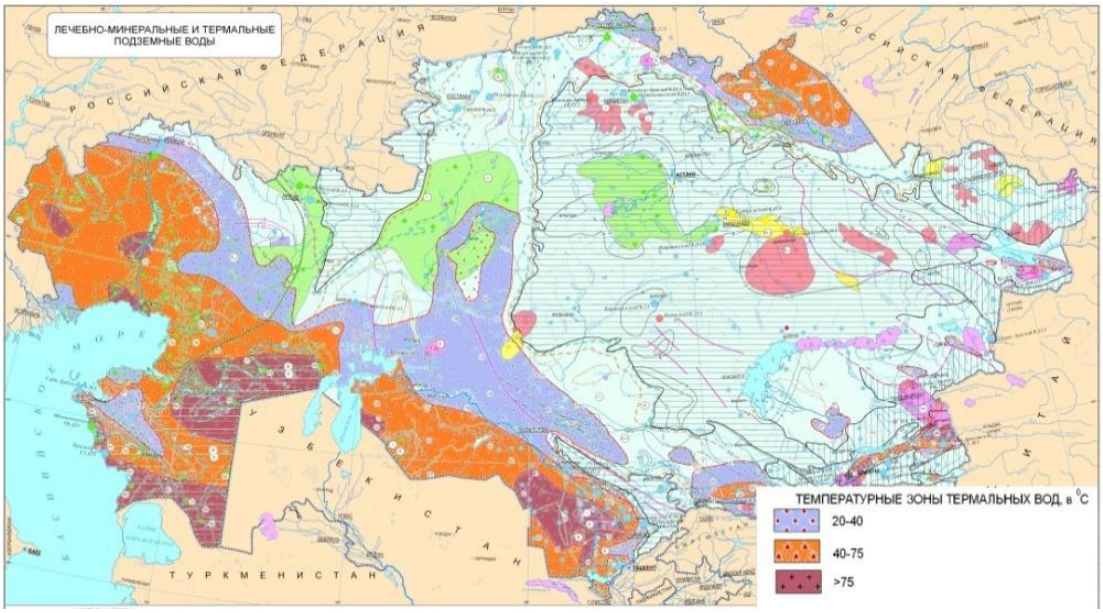

Figure 8: Annual wind speed distribution in Kazakhstan

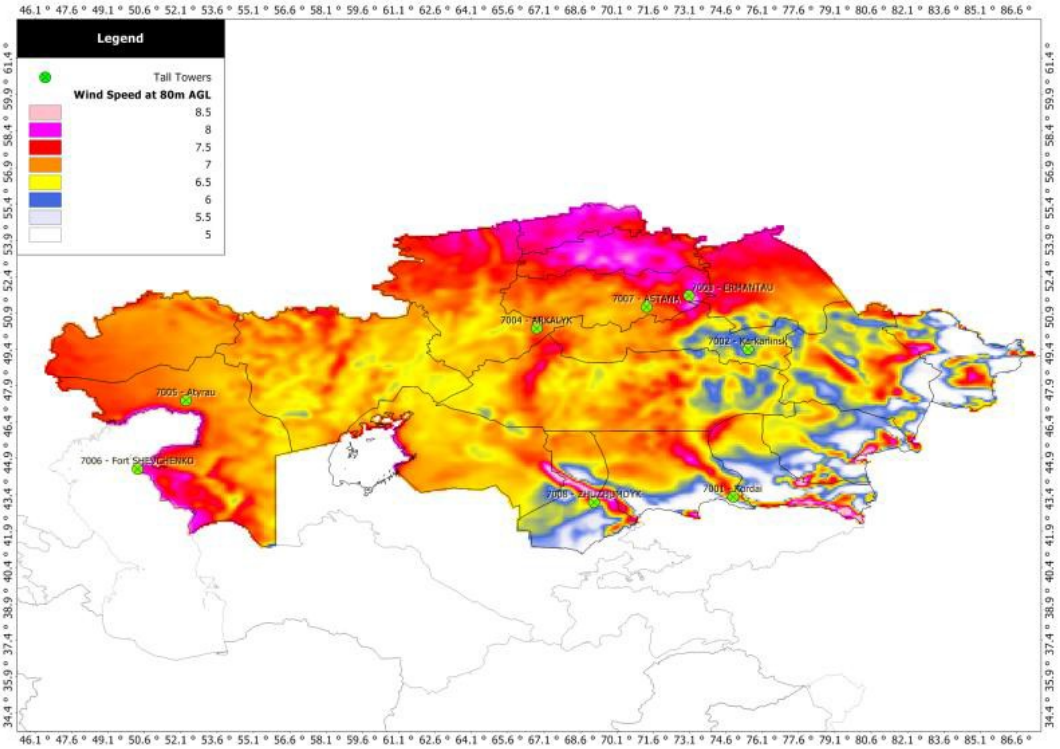

A UNDP report on wind power potential in Kazakhstan**[7]** shows that the annual wind speed in Kazakhstan is over 7 m/s which is ideal for wind farm statistically speaking.

From above, we can safely draw a conclusion that clean power has a strong outlook in Kazakhstan and in order to make the most of it, the government should take measures to develop both the solar power field, in the southern part of the country, wind power field in the central and northern region and hydropower dam in the east.

2. Literature Review

From fluid mechanics we know that the kinetic power of air flow can be expressed as below:

$$E=\frac{1}{2}\rho A v^3 \qquad \text{Eq (1)}$$

Where ρ is the density of air, A is the area of airflow, v is the velocity of air flow.

The wind turbine is a device that converts the kinetic power of air flow into the mechanical power of the wind turbine which will drive the generator and finally generate electrical energy, which means that the electrical power originates from the kinetic energy loss of the air flow through the wind turbine. When air flows over the wind turbine blade, which is similar to the wing of a plane, the change of direction of air flow velocity causes a difference in pressure which generates lifting force to make the wind turbine rotate. However, lifting force is not the

only form of force that emerges in this process, there is also drag force and pitching moment.

Figure 9: Oriol Lehmkuhl-simplified methods for wind turbine blade design

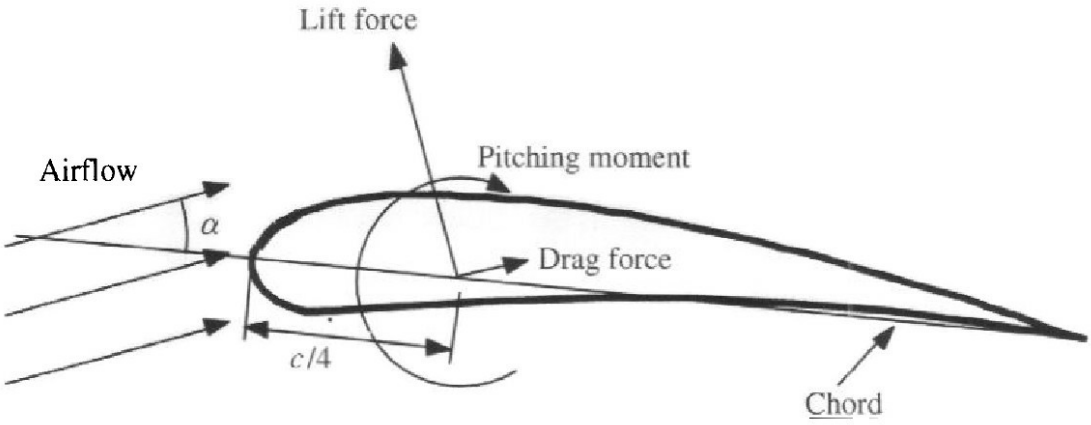

The lift and drag force vary with angle of attack (AoA) as shown below. When AoA exceeds certain range it will lead to separation of boundary-layer and cause turbulence which will increase drag force dramatically. Therefore the key to achieving maximum torque is to choose the ideal AoA to suit the wind speed.

Figure 10: Lift and drag coefficient vs angle of attack

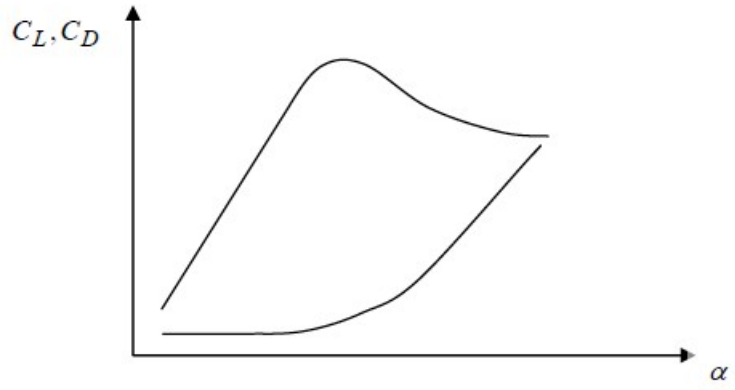

Figure 11: stall development

Stall:

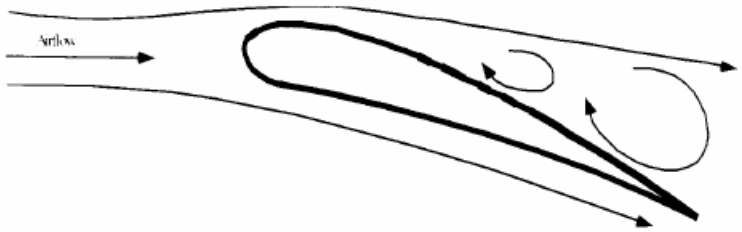

The actual airflow motion is complicated, there is a limit (Betz limit) to the efficiency of the wind turbine with a theoretical maximum of 0.593(Betz Limit) **[8]**. And there is the expression for power output:

$$P=\frac{1}{2}Cp*\rho A v^3 \qquad \text{Eq (2)}$$

Where C_p is the power coefficient and A is the blade swept area. As a matter of fact, the power coefficient varies when it comes to different tip speed ratio (TSR) which is the ratio of tip speed of the rotor to free wind speed. And every power coefficient value has its corresponding unique tip speed ratio. Therefore, the only way to seek an improvement of power coefficient is to make a more detailed design of the wind turbine blade. Yet, in the wind turbine industry, the improvement achieved by detailed design is only considered modest and the main approach to get higher power output is to increase the length of the blade, which is recognized as the simplest and most effective avenue to achieve the goal.

2.1 Different Types of Wind Turbines

Modern wind turbines can be classified into two types considering the arrangement of the rotor. Turbines rotate about a horizontal axis are called Horizontal-axis wind turbines(HAWT). Wind turbines that rotate about a vertical axis instead of the horizontal axis are classified as Vertical-axis wind turbines(VAWT). Horizontal-axis wind turbines are more common and have a longer history compared to Vertical-axis wind turbines. Moreover, in terms of efficiency and power output, horizontal-axis wind turbines perform better than vertical ones **[9]**.

The structure of Horizontal-axis wind turbines and Vertical-axis turbines differ. They can be with or without blades. The former have the main rotor shaft and generator installed at the top of a tower, the height of the tower can exceed 100 metes in order to catch the wind with higher velocity, and the turbine must be pointed into the wind to get the maximum efficiency. However, in some regions, the direction of the wind changes, therefore, servomotors are applied to the joint between the tower and the disc to control the direction of the turbine. In terms of the position of the turbine, most turbines are placed in front of the

tower while some others are placed behind the turbine. The turbine blades are required to be rigid enough when placed in front of the tower on account of the deformation caused by wind with high velocity that can bend the blades and sometimes the bent blade can hit the tower. However, if the turbine is placed behind the tower, then the blades are allowed to be flexible though it will reduce the blade swept area. And the commonly used wind turbines in commercial wind farms have the structure with three blades that are considered the most reliable due to low torque ripple and cost-efficient design.

Vertical-axis wind turbines(VAWT) have the turbine arranged vertically and due to the vertical axis arrangement, this type of wind turbines do not require an extra mechanism to point the turbine towards the wind. The vertical-axis turbines can work even if sited in an area where the direction of the wind velocity is highly variable, which is an advantage compared to horizontal-axis wind turbines **[10]**. Also, due to the structure of vertical -axis wind turbines, the generator and other components can be placed close to the ground, which makes the maintenance and repair of the wind turbine much easier compared to horizontal-axis wind turbines that sometimes can reach a height of over 100 meters and also makes it possible to install them on the skyscrapers that are commonly higher than 100 meters. Thus, the construction and installation of the vertical-axis wind turbines are also much more convenient. However, vertical-axis wind turbines produce less energy compared to horizontal ones, which is also the major drawback of this design. There are also subtypes originate from the vertical axis design such as “Darrieus wind turbine” **[11]** and “Giromill”**[12]**. Darrieus wind turbines, so-called “Eggbeater” wind turbines, have satisfactory performance in terms of efficiency,
but the large torque ripple and cyclical stress produced by the rotor on the wind tower can cause different types of failures thus the reliability of this design is poor. Also, this design requires an external force to start turning due to the low starting torque, which means there has to be the external power supply to start the turbine **[13][17].** On the contrary, Giromill design, with straight blades, is self-starting and has lower bending stress on blades.

When it comes to starting wind speed, horizontal axis wind turbines require a wind speed of 4-5 m/s and sometimes 5.9m/s**[14]**, which is not satisfactory. On the contrary, vertical axis wind turbines demand smaller starting wind speed and some vertical axis wind turbines are self-starting, which is an advantage compared to horizontal axis design.

Considering the effects on the environment, large wind farms of hundreds of horizontal axis wind turbines generate noise that can affect the normal activities of local animals and the high speed rotating blade can kill or injure flying birds. On the other hand, vertical turbines can be installed on the rooftop of high buildings in cities and have less impact on the natural environment.

2.2 Design and Construction of Wind Turbines

There are three aspects of wind turbine design. The first is the design of the wind turbine structure, including the arrangement of turbines and the placing of components. The second is the blade design optimization which requires building a numerical aerodynamic model and geometric model, simulation and wind tunnel tests, which will be different if the wind turbine is bladeless. The third is material design since the material defines the properties of the blade and also affects the fluid-structure interaction performances. Furthermore, the right material can also reduce the construction and maintenance cost and in return lower the price of electricity generated from wind farms.

The commonly used structure, three-bladed horizontal axis, is considered the most efficient and reliable design. However, some innovative structural design may lead to a breakthrough in the utilization of wind power. Also, the optimization design of the machinery and control system can contribute to better performance and lower cost **[15,19]**.

The material of wind turbine blades defines the properties of the blade. With the development of material science and engineering, a growing number of new materials were designed to meet different requirements. Composite materials have low density and high strength compared to conventional materials and is an ideal choice for the construction of wind turbines. Currently, glass fiber and composite materials with high strength are used in constructing large commercial wind turbine blades.

The blade design optimization is the key to achieve better performance and also the most challenging part of wind turbine optimization since the airflow is far more complicated than theoretical assumption and the interaction between airflow and blade varies along the blade in the direction of the span. Thus advanced computational methods should be applied. Ansys and Workbench are commonly used in the numerical simulation of different engineering problems. Also, in some research, the use of NACA airfoils, Xfoil and AirfoilPrep are combined with Matlab to generate the aerodynamic model of the blade and simulation. The key to blade design optimization is to determine the angle of attack (AoA) in every different section to get an ideal lift and drag coefficient. The twist and change in thickness along the direction of the span are also crucial to reach the goal. A common method is to divide the blade into several sections and calculate the twist angle and thickness change per unit span. An aerodynamic model, an optimization algorithm and a geometric modeler constitute the basic physics-based aerodynamic optimization method, and a structural dynamics model might be needed if structural design optimization is required.

2.3 Basic Theories and Methods of Wind Turbine Design Optimization

Blade Element Momentum theory is the most applied technology in blade aerodynamic analysis, the purpose of this theory is to estimate the load of airflow, which is crucial to the design optimization **[16]**.

The Glauert method and Wilson method are the most preferred and accurate methods applied in blade aerodynamic design. Glauert method is based on Blade Element Momentum theory, and it takes the flow of rear vortex into consideration and also includes a and a' factors. But this method ignored the effect of drag and tip loss.

The Wilson method not only includes the effects of tip loss and drag on blade aerodynamic performance, but also takes none-design working condition into consideration. In other words, the Wilson method is based on the Glauert method, but more comprehensive and accurate. Furthermore, the model of the Wilson method is much simpler and easy to calculate **[20]**.

2.4 Latest Work in Wind Turbine Optimization

Various studies have been conducted for the optimization of wind turbine blades, most of which are 2D optimization or 2.5D optimization. Those studies focus on the impact of baseline foils that are used to determine the entire geometry of the blade, and the effect of the rotational field and radial velocity are not taken into consideration. Only a few pieces of research are actual 3D optimization.

In Naishadh's research **[21]**, a multidisciplinary design optimization process is defined to optimize both aerodynamic and structural performance using response surface optimization tool in Ansys Workbench Design Xplorer. A fluid-structural interaction system is developed in order to maximize aerodynamic efficiency and structural robustness, in which the blade mass and cost are constrained. The result is an optimal blade model with maximum power output and minimum weight while meeting the required structural strength. However, the aerodynamic performance prediction in the optimization process is performed in Xfoil/Qblade, which means the aerodynamic optimization is still in 2D, so the entire optimization is actually a 2.5 D optimization. In addition, the power output only increased by around 3 percent, while the total cost of the blade also increases by 1.5 percent. In conclusion, this optimization is not very successful.

On the contrary, in Tristan's study **[22]**, in which the torque is maximized by an optimization framework, consisting of a RANS CFD model coupled to sparse nonlinear optimizer which is a sequential quadratic programming algorithm. The results show an increase up to 20 percent in torque. However, the overall computing time is very long, up to over one day using 256 processors. Moreover, the CFD validation is doubtful because the geometry is changed significantly in order to achieve convergence, which means the turbulence model selected in the simulation might be wrong.

An aerodynamic shape optimization method is proposed in Ozge's research using a parallel genetic algorithm **[23]**. The methodology is based on BEM theory and genetic algorithm. Similar to Naishadh's study, the aerodynamic performance is also conducted in Xfoil. In this study, the baseline foil shape which determines the entire blade geometry is optimized by genetic algorithm to

achieve maximum power output while the thickness is constrained. And the power output increased by 10 percent. However, BEM theory has certain limitations and is not considered as reliable in studying the aerodynamic performance of a wind turbine, which is discussed in this thesis.

Combining artificial neural network and CFD simulation, Elfarra carried out optimization research which includes winglet optimization **[24]**. In his study, the twist angle, pitch angle as well as the winglet configuration are set as design parameters. The optimization is based on CFD simulation results and the optimization process is done by genetic algorithm where the objective function is approximated in artificial neural network by CFD data samples, which means this methodology largely relies on the accuracy of initial CFD simulation results. The result shows a 38 percent increase in power output. Though the CFD prediction of the base model is inaccurate under high wind speed condition, which makes the final result questionable, the optimization methodology provides a new approach to perform optimization on a larger scale.

2.5 Goal and Scope of Current Research

The purpose of this study is to propose, practice and validate a novel way of design optimization for wind turbine blades to achieve greater power output for one wind turbine. In the optimization process, a parameterized wind turbine rotor model is built. And on the basis of a 3D URANS transient CFD study where the power output is taken as an output parameter, the geometry is changed to maximize the power output. In addition, this study is mainly an exploration of a new and much-simplified approach to design and optimize wind turbines which can be also used in other airfoil design optimization processes. The scope of this research is to conduct an optimization process in which the adjustable trailing edges on 20 cross-sections are set as design parameters. Combining the CFD results and the built-in optimization tool in ANSYS, instead of establishing an integrated framework that consists of different software interfaces as is in other studies, the optimization is conducted to maximize the power output of the NREL phase VI blade under 10m/s wind speed condition. Moreover, this study proves the feasibility of a less computation expensive optimization method compared to existing methodologies.

3. Fundamental Theories

3.1 Basic Theories

The design optimization of a wind turbine blade has a significant effect on the aerodynamic performance of the wind turbine. So far, Blade Element Momentum (BEM) theory is the most used theory in wind turbine blade aerodynamic analysis.

3.1.1 Momentum Theory and Betz's Limit

The Momentum Theory, or disk actuator theory, is a theory that was established to describe a mathematical model of an ideal actuator disk, such as an airplane propeller or a helicopter rotor or a wind turbine rotor in this case, by W.J.M Rankine in 1865 and later refined by Alfred George Greenhill in 1888 and Robert Edmund Froude in 1889 **[25].** In this theory, the rotor is modeled as an infinitely thin disk, in which a constant velocity along the axis of rotation is induced. And a flow around the rotor is created by this disk. A mathematical connection between power, the radius of the rotor, torque and induced velocity can be extracted under a series of certain mathematical premises of the fluid. However, in this theory friction is not included. The relationship between power and thrust for a stationary disk or rotor like a wind turbine can be simply expressed as

$$p=\sqrt{\frac{T^3}{2\rho A}} \qquad \text{Eq (3)}$$

where :

- T is the thrust
- ρ is the density of the fluid
- A is the area of the thin disk

Though seems quite simple and clear, the theory itself is based on several assumptions:

- There is no resistance from the infinitely thin disk to passing air flow
- 1-D analysis only
- Both the thrust and velocity are uniformly distributed over the disk
- Both far upstream and far downstream are free flow with static pressure
- The fluid has no viscosity and is incompressible

Figure 12: Control volume

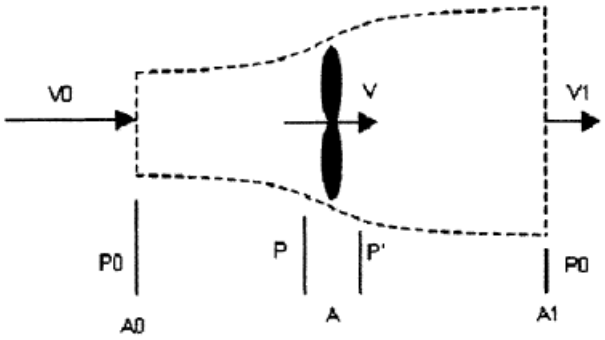

After applying the law of conservation of mass, there is

$$V_0 A_0 = VA = V_1 A_1 = V_i A_i = \dot{m} \qquad \text{Eq (4)}$$

Where i stands for far upstream.

And by momentum equation there is :

$$T = \dot{m}(V_0 - V_1) = \rho AV(V_0 - V_I) \qquad \text{Eq (5)}$$

Where:

- $\dot{m}$ is mthe ass flow rate of air
- V is the velocity of air flow at A
- V_0 is the velocity of air flow before the disk
- V_1 is the velocity of air flow after the disk

Then by applying the Bernoulli equation, we can get:

$$p - p' = \frac{1}{2}\rho(V_0^2 - V_1^2) \qquad \text{Eq (6)}$$

Where :

- p is the static pressure before the disk
- p' is the static pressure after the disk

So thrust can be expressed as

$$T = A(p - p') = \frac{1}{2}A\rho(V_0^2 - V_1^2) \qquad \text{Eq (7)}$$

By applying the continuity equation, the force can be written as

$$\begin{aligned} F &= ma \\ &= m\frac{dV}{dt} \\ &= \dot{m}\Delta V \\ &= \rho AV(V_1 - V_2) \end{aligned} \qquad \text{Eq (8)}$$

The power of wind can be expressed as

$$\begin{aligned} P &= F \cdot V \\ &= \rho \cdot A \cdot v^2 \cdot \text{¿} \end{aligned} \qquad \text{Eq (9)}$$

Since power can be calculated in another way by introducing kinetic energy, there is

$$P = \frac{\Delta E}{\Delta t}$$

$$= \frac{1}{2}\cdot \acute{m}\cdot\left(V_1^2 - V_2^2\right) \qquad \text{Eq (10)}$$

And by equating these two equations yields:

$$V = \frac{1}{2}\left(V_1 + V_2\right) \qquad \text{Eq (11)}$$

Which means the wind speed at the device is the average of wind speed before and after the device. And by differentiating $\acute{E}$ with respect to V_2/V_1 , the maximum power that can be extracted from wind can be expressed as :

$$P_{max} = \frac{16}{27}\cdot\frac{1}{2}\cdot\rho\cdot A\cdot V_1^3 \qquad \text{Eq (12)}$$

Which indicates that the maximum value of energy that can be extracted from wind has a limit which is 16/27 or 59.3%. And this is called the Betz's Limit **[26].** Modern large commercial wind turbines can achieve maximum values for power coefficient from 75% to 85% **[27].**

3.1.2 Blade Element Theory

In 1878, William Froude originally designed a mathematical process in order to determine the aerodynamic behavior of propellers **[28].** In this theory, the blade is divided into several small sections to calculate the forces on each of these sections which are called blade elements. Then the forces on the entire blade can be computed by integrating the forces on each element along the blade. However, there are major difficulties including modeling the induced velocity over the rotor or disk. Therefore, blade element theory cannot be used unless combined with momentum theory.

Figure 13: Forces and velocities for a blade element

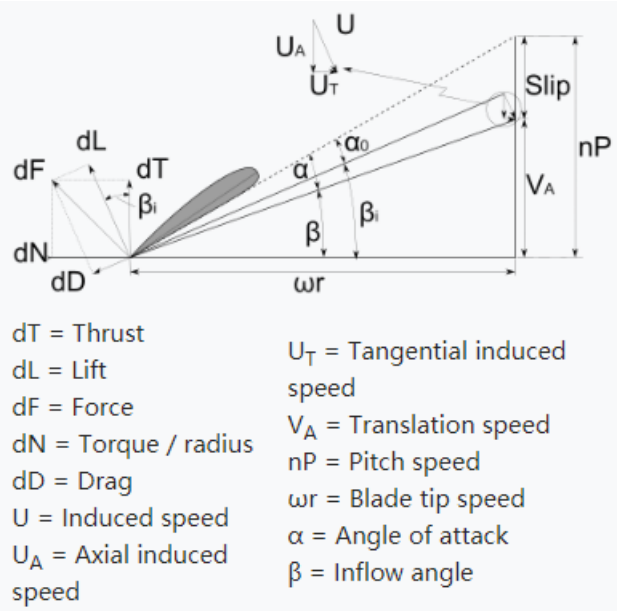

3.1.3 Blade Element Momentum Theory

Blade Element Momentum Theory (BEM) is attained by combining blade element theory and momentum theory due to the difficulties of blade element theory in calculating induced velocities on a rotor **[29].** The BEM is not reliable when it comes to simulating the aerodynamic load distribution on the turbine blade especially for stalled and yawed rotor conditions**[30]**. Moreover, the impact of dynamic stall on the lift coefficient results in inaccurate results for unsteady BEM **[31]**. So far, various correction methods such as hub loss correction **[32]**, skewed wake correction **[33]**, Glauert **[34]**, tip loss correction **[35]**, 3D correction **[36]** and Buhl empirical corrections **[37]** have been proposed to improve the reliability of BEM method.

4. CFD Analysis and Optimization of Wind Turbine Blades

4.1 Inverse Blade Element Momentum Theory (IBEM)

This thesis carefully studied the automated optimization framework by Sagi. **[38]** The automated framework combined Solidworks, Ansys, and Matlab. The 3D parametric blade model is linked to an external file which can be manipulated in Matlab by scripts. The external file which determines the 3D model will rebuild the 3D model in Solidworks then put in Ansys Fluent for CFD simulation. The simulation results are optimization targets in Matlab. In this case, the power output is the optimization target and the wist angles of 20 individual sections are the variables that will be changed automatically in order to find the optimum design which offers the maximum power output. However, the framework is not adopted because the latest version of ANSYS has its own optimization tool which is similar to that framework and, most importantly, is much simpler and user-friendly. The toolbox is called Design Xplorer. The module used in this research is called Direct Optimization where the global variables set in the Solidworks are set as input parameters and the power output obtained from the simulation results is set as the output parameter. The output parameter is the single optimization objective which is to be maximized in the optimization process.

4.2 CFD Study of NREL PHASE VI Rotor

Accurate simulation results are crucial to validate the CFD model which can then be used in the optimization process. In order to have more accurate results, a transient study is committed in the numerical simulation process. Ansys Fluent provides the simulation platform, where the whole rotor model within a certain domain is established. And a sliding mesh method is adopted, which contains a cylindrical rotor mesh rotating with the rotor and a cylindrical stationary stator mesh surrounding the rotator mesh. And the two meshes have a sliding interface. The rotor model is subtracted from the cylindrical rotating mesh body.

4.2.1 Governing Equations

In this thesis, a transient CFD study was conducted using the sliding mesh method instead of the rotating frame method that is commonly used in steady state CFD studies of wind turbines. Because of this, the turbulence model must be carefully selected.

When considering unsteady airflow over a rotating blade, the 3D turbulence is very complex and difficult to calculate. Therefore, a k-epsilon model with standard near wall treatment is selected.

The realizable k-epsilon model is one of the RANS (Reynold-averaged Navier-Stokes) turbulence models.

The governing equations for the CFD simulation utilizing 3D Reynolds-Averaged Navier-Stokes (RANS) equations are formulated as follows:

Conservation of mass:

$$\frac{\partial \rho}{\partial t}+\nabla\cdot(\rho \acute{U})=0 \qquad \text{Eq(13)}$$

Conservation of momentum:

$$\frac{\partial(\rho \acute{U})}{\partial t}+\rho(\acute{U}\cdot\nabla)\acute{U}=-\nabla p+\nabla\cdot\acute{\sigma}+\rho \acute{f}_b \qquad \text{Eq(14)}$$

where

$\acute{\sigma}$ is the stress tensor for Newtonian viscous fluid

$\acute{f}_b$ are body forces,i.e. gravity

the bar as in $\acute{U}$ means that U is a vector

Equation (13) is the 3D unsteady continuity equation at a point in a compressible fluid. The term $\frac{\partial \rho}{\partial t}$ represents the rate of change in time of the density and $\nabla\cdot(\rho \acute{U})$ is called the convective term which describes the net flow of mass out of the element across its boundaries **[39].**

All air flows in this thesis are considered incompressible, which means the density of the fluid, air, is constant. Also, the impact of temperature is ignored, and the conservation of internal energy is not included in the governing equations in this chapter.

Since the density of the incompressible fluid is constant, equation (13) becomes

$$\nabla(\rho \acute{U})=0 \qquad \text{Eq(15)}$$

or be represented in Cartesian notation as

$$\frac{\partial u}{\partial x}+\frac{\partial v}{\partial y}+\frac{\partial w}{\partial z}=0 \qquad \text{Eq(16)}$$

by implementing equation (15), equation (14) can be simplified as**[40]**

$$\frac{\partial(\rho \acute{U})}{\partial t}+\rho(\acute{U}\cdot\nabla)\acute{U}=-\nabla \rho+\mu\nabla^2\acute{U}+\rho \acute{f}_b \qquad \text{Eq (17)}$$

If the flow is steady state then the first term on the left is equal to zero, but the present thesis studies transient flow so the term is kept in the equation.

The RANS model, compared with LES (Large Eddy Simulation) and DNS (Direct Numerical Simulation), is most commonly used to calculate turbulence because it provides the most economical approach in the calculations of complex turbulent flows but these set of equations assume that the flow is incompressible. Different from other models, there is an alternative formulation for the turbulent viscosity in the realizable k-epsilon model. In addition, from an equation for the transport of the mean-square vorticity fluctuation, a modified transport equation for the dissipation rate has been derived. The realizable k-epsilon model can be represented as in equation (18),(19):

$$\frac{\partial}{\partial t}(\rho k)+\frac{\partial}{\partial x_j}(\rho k u_j)=\frac{\partial}{\partial x_j}\left[\left(\mu+\frac{\mu_t}{\sigma_k}\right)\frac{\partial k}{\partial x_j}\right]+G_k+G_b-\rho\varepsilon-Y_M+S_k$$

Eq (18)

$$\frac{\partial}{\partial t}(\rho\varepsilon)+\frac{\partial}{\partial x_j}(\rho\varepsilon u_j)=\frac{\partial}{\partial x_j}\left[\left(\mu+\frac{\mu_t}{\sigma_\varepsilon}\right)\frac{\partial \varepsilon}{\partial x_j}\right]+\rho C_1 S_\varepsilon-\rho C_2\frac{\varepsilon^2}{k+\sqrt{v\varepsilon}}+C_{1\varepsilon}\left(\frac{\varepsilon}{k}\right)C_{3\varepsilon}G_b+S_\varepsilon$$

Eq (19)

Where

$$C_1=max\left[0.43\frac{\eta}{\eta+5}\right],\eta=S\frac{k}{\varepsilon},S=\sqrt{2S_{ij}S_{ij}}$$

G_b is the generation of turbulence kinetic energy due to buoyancy

Y_M represents the contribution of the fluctuating dilatation in compressible turbulence to the overall dissipation rate

C_2 and $C_{1\varepsilon}$ are constants

σ_k and σ_ε are the turbulent Prandtl numbers for k and ε, respectively

S_k and S_ε are user-defined source terms.

And form equation (20) yields the eddy viscosity

$$\mu_t=\rho C_\mu\frac{k^2}{\varepsilon} \qquad \text{Eq (20)}$$

However, C_μ is not a constant as in other k-epsilon models. C_μ is derived from equation (21) instead.

$$C_\mu=\frac{1}{A_0+A_s\frac{kU^{\acute{}}}{\varepsilon}} \qquad \text{Eq (21)}$$

Where

$$U^{\acute{}}=\sqrt{s_{ij}s_{ij}+\widetilde{\Omega}_{ij}\widetilde{\Omega}_{ij}}$$

$\widetilde{\Omega}_{ij}$ represents the mean rate-of-rotation tensor with angular velocity ω_k .And constants A_0 and A_s are computed from equation (22).

$$A_0=4.04,A_s=\sqrt{6}\cos\phi \qquad \text{Eq (22)}$$

Where

$$\phi=\frac{1}{3}cos^{-1}(\sqrt{6}W)\ ,\ W=\frac{s_{ij}s_{jk}s_{ki}}{\tilde{s}^3}\ ,\ \tilde{s}=\sqrt{s_{ij}s_{ij}}\ ,\ s_{ji}=\frac{1}{2}\left(\frac{\partial u_j}{0x_i}+\frac{\partial u_i}{\partial x_j}\right)$$

4.2.2 Numerical Methods and Boundary Conditions

The numerical method utilized in this study in CFD simulation in ANSYS FLUENT. Considering the incompressible nature of the flow, a pressure-based absolute transient study is carried out, using the finite-volume method for space discretization and semi-implicit time integration of the SIMPLEC solver of Patankar [52] on 16 CPU cores and the second order upwind option is chosen for pressure, momentum, turbulence kinetic energy. The k-epsilon turbulence model is chosen where the standard near wall treatment function is selected. And since the sliding mesh method is adopted in mesh configurations, a mesh motion with 72 rpm angular velocity is assigned to the rotor domain which is shown in Figures 15 and 16. In boundary conditions, the inlet is chosen as velocity inlet and the wind speed is 10m/s normal to the boundary. The cylindrical surface is

set as symmetry, which means there is no velocity component that is normal to the cylindrical boundary.

4.2.3 Mesh Convergence Study and Validation of CFD Model

Figure 14: S809 foil shape of the NREL phase VI wind turbine

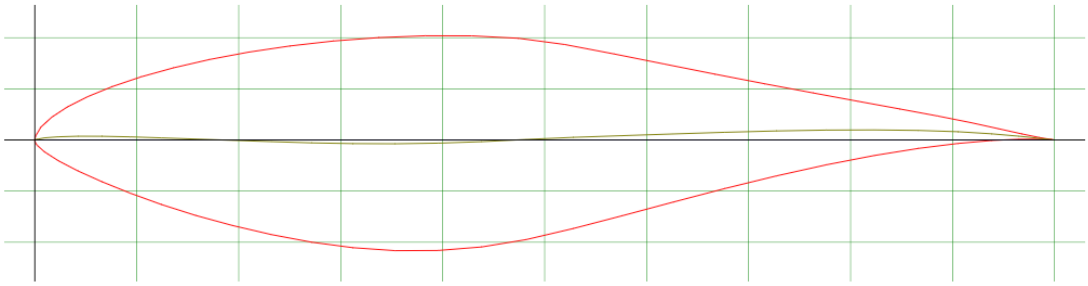

Figure 15: Simulation geometry in ANSYS FLUENT

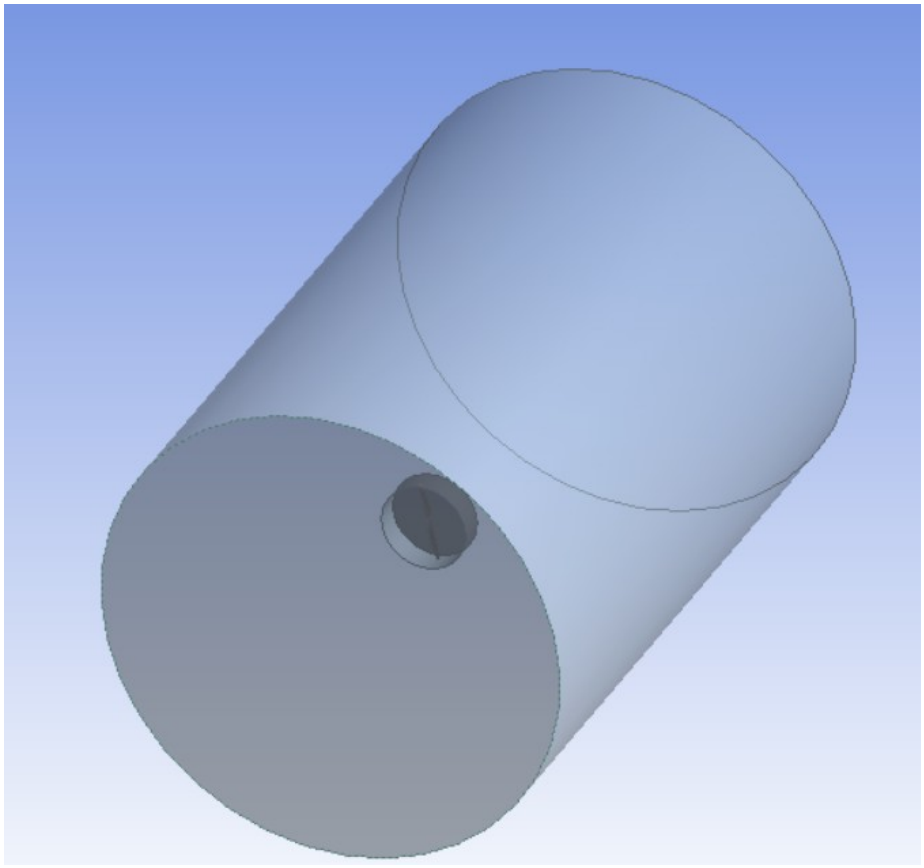

Figure 14 shows the S809 airfoil used for the NREL blade. In the sliding mesh method, the larger cylinder mesh body in Figure 15 is named stator, and the inner mesh disk is called rotor. The blades are subtracted in Boolean from the rotor disk (see Figure 16).

Figure 16: Rotating domain

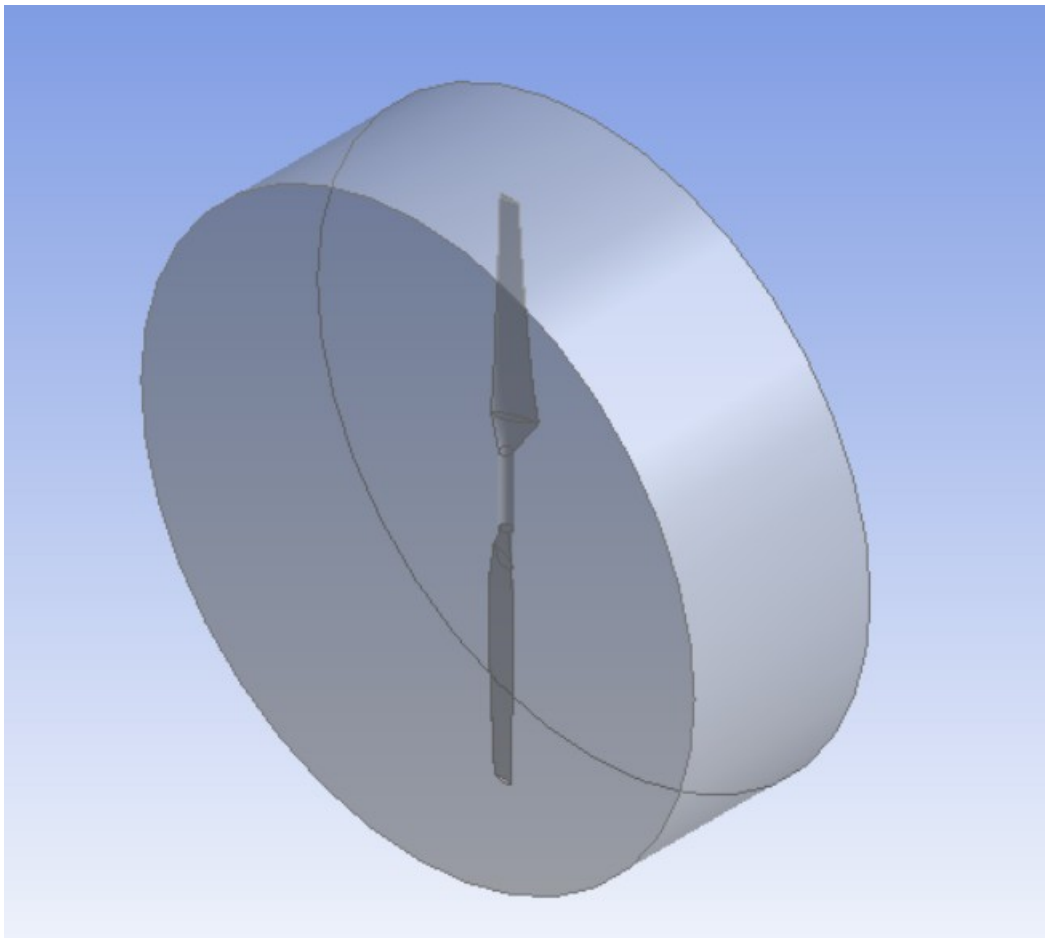

Figure 17: Mesh around blade surface

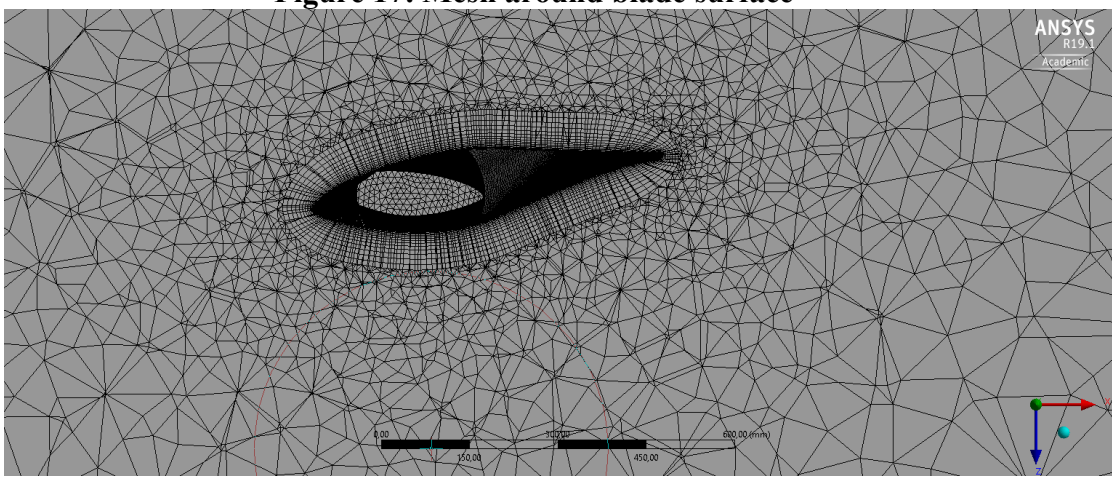

4.2.3.1 Mesh Convergence Study

Different meshes with different mesh densities are used to find out the optimal mesh that should be used in order to achieve high accuracy and at the same time make the simulation process less time-consuming and mesh independent. In addition, a series of CFD simulations have been conducted, where the pressure coefficient at different positions are used as criteria to evaluate the accuracy of the simulation. Some sample results are shown below. All simulations meet the accuracy requirement that the residuals should be smaller than 0.001.

Figure 18: CFD calculation residuals

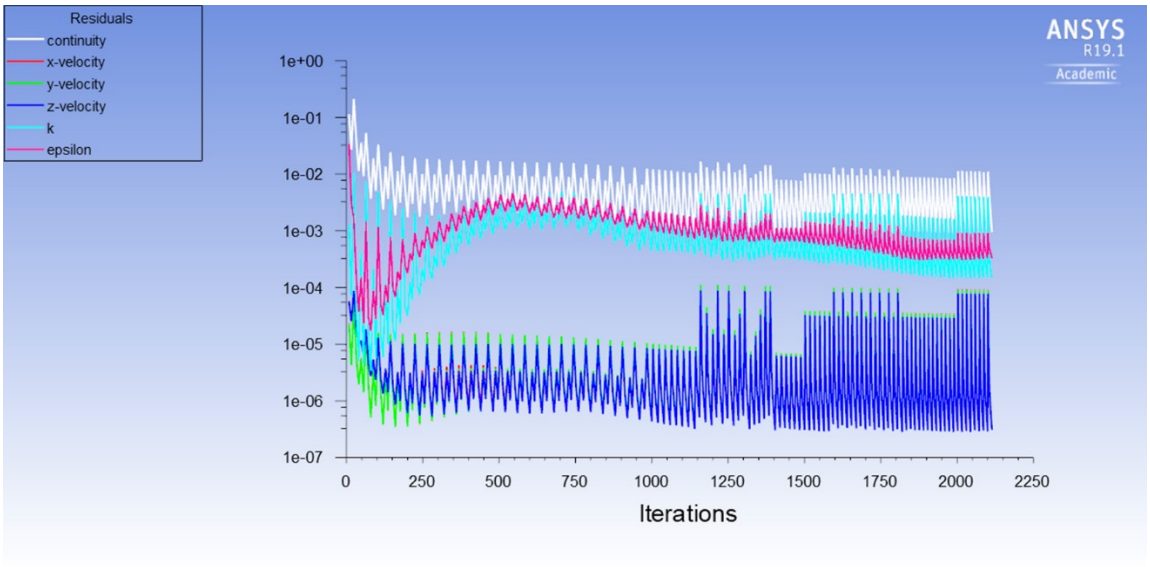

To show the convergence of the CFD method in this research, a mesh refinement study based on several different meshes was conducted for the NREL phase VI turbine rotor for 10m/s wind speed.

Figure 19: results of mesh refinement study

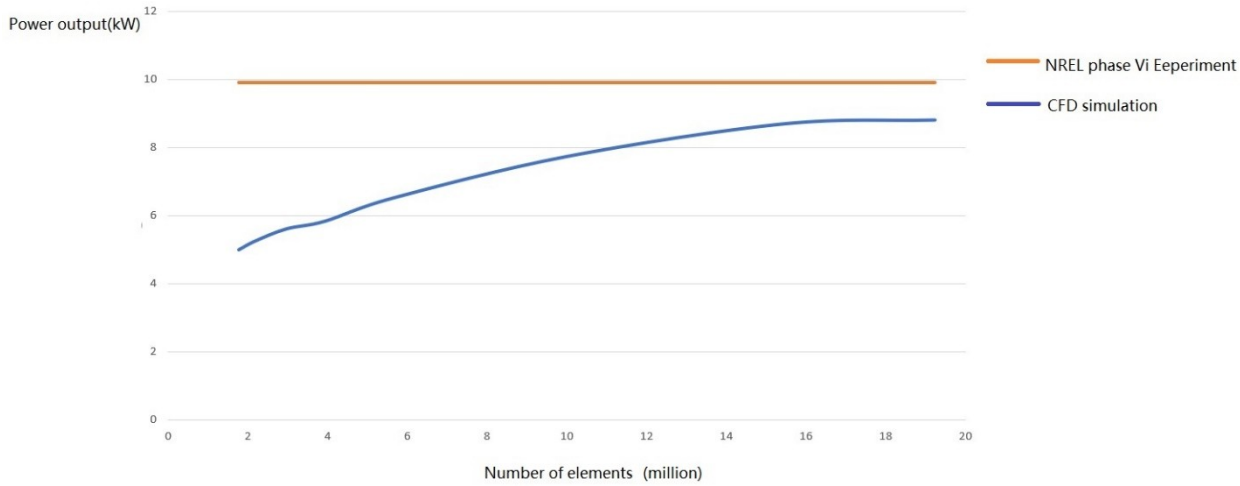

Figure 19 shows that the simulation result can be improved by refining the mesh. In addition, convergence occurs when computational element number exceeds 17 million. Unfortunately, the power output is 10 percent lower than the given experimental data so the pressure coefficient is used as a criterion to verify the accuracy of CFD simulation. The simulation used in verification contains 19.2 million elements, the global mesh sizing is 600mm and the blade surface sizing is 7 mm. First layer thickness is chosen as inflation option as in all the other simulations, where first layer height is set as 1mm, the growth rate is

1.2 by default and 15 layers are established.

4.2.3.2 Validation of CFD Results and Model

The results at 30 percent span in Figure 20 shows good accuracy on the pressure surface where the curve is not beyond the experimental data range. On the other hand, the pressure coefficient on the suction surface near the leading edge is lower than the mean value of experimental data which is still within the experimental data range.

Figure 20: pressure coefficient at 30 percent span

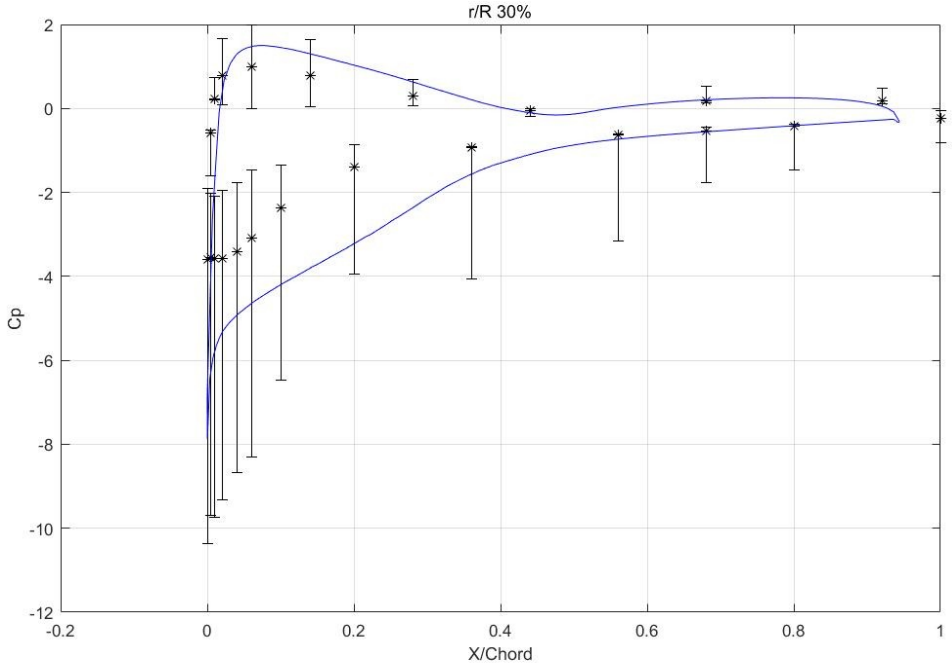

Figure 21: pressure coefficient at 47 percent span

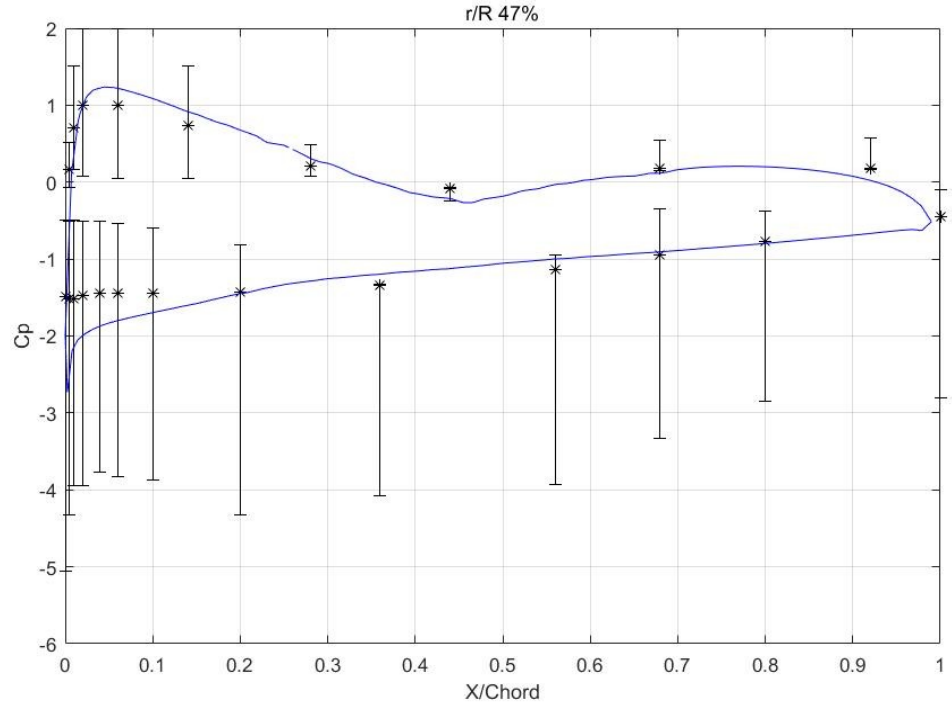

Figure 21 shows good accuracy in the simulation results at 47 percent span. The results are close to the experimental mean value and at the same time within

the data range except for one single point on the suction surface located at 0.36 on the x coordinate.

Figure 22: pressure coefficient at 63 percent span

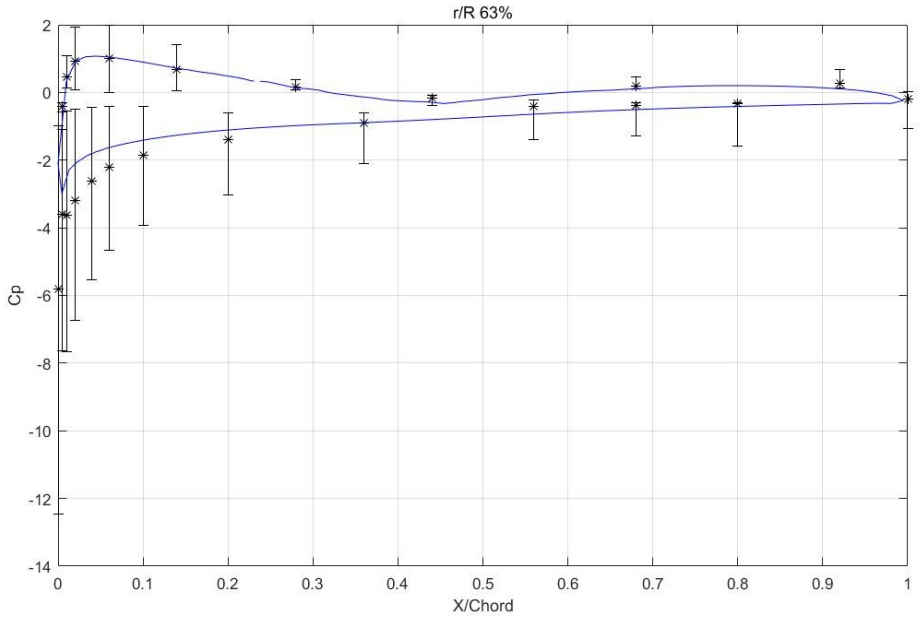

At 63 percent span, as shown in Figure 22, the simulation results also in good accordance with experimental data. It can be observed that most of the mean values are on the simulation curve and slight deviation only occurs near the leading edge on the suction surface.

Figure 23: pressure coefficient at 80 percent span

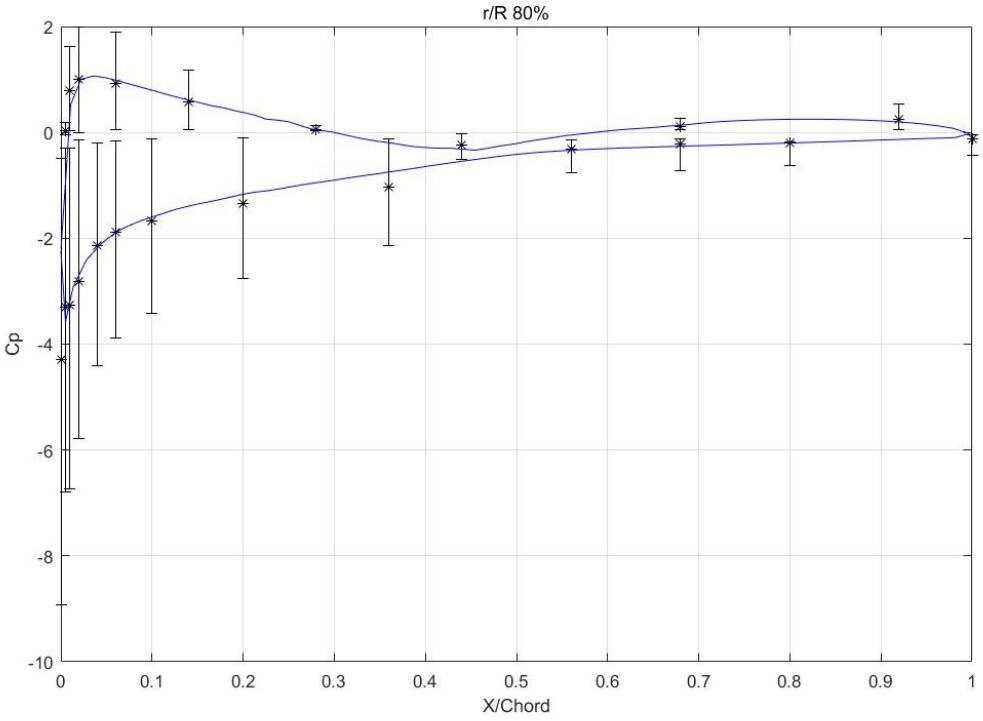

Figure 23 shows high accuracy at 80 percent span, where almost every mean value is on the simulation curve.

Figure 24: pressure coefficient at 95 percent span

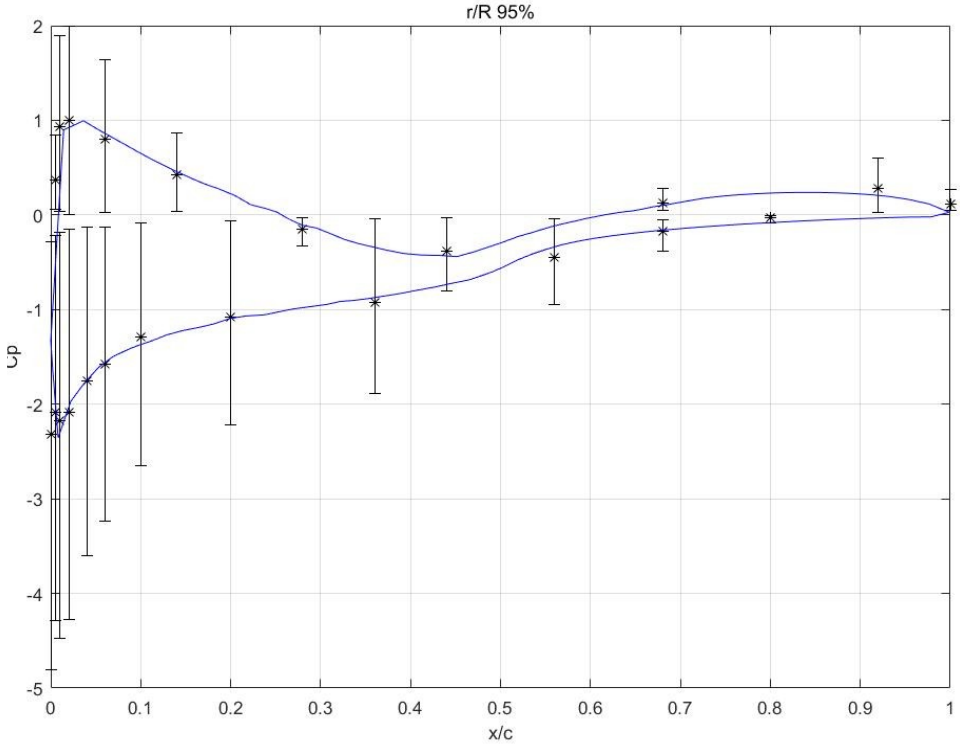

Similar to the results at 80 percent span, Figure 24 shows high accuracy in the simulation results. And average Y plus is 32.5, which is suitable for K-e model.

Figure 25: wall Y plus contour

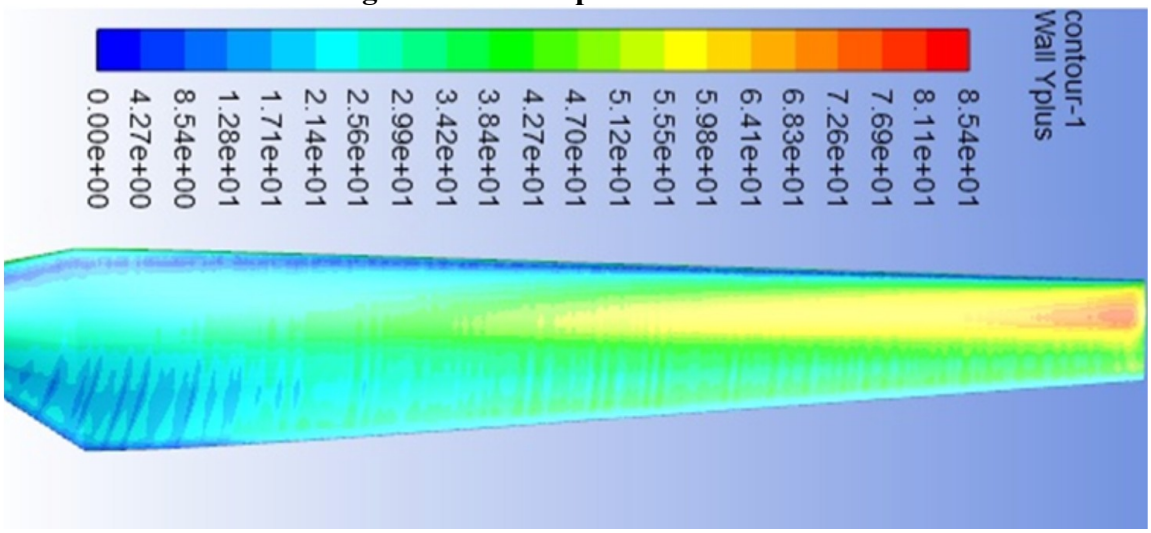

In conclusion, the CFD simulation results can be safely considered as accurate and the simulation settings can be introduced into the optimization system. However, it cannot be denied that the 30 percent span results have some issues.

The results verification uses pressure coefficients as the main criteria. As shown in the figures above, pressure coefficients are in good agreement with the experimental data, all the mean values of pressure coefficient are close to the curve and the simulation results do not exceed the boundary of experimental data that is represented as a bar in the graph. However, the results at 30 percent span are not very close to experimental data. The possible reason is that the position is too close to the hub where, in the experiment, the measurement

device is installed. The experimental system is shown below in Figure 25.

Figure 26: NREL NASA experiment turbine components

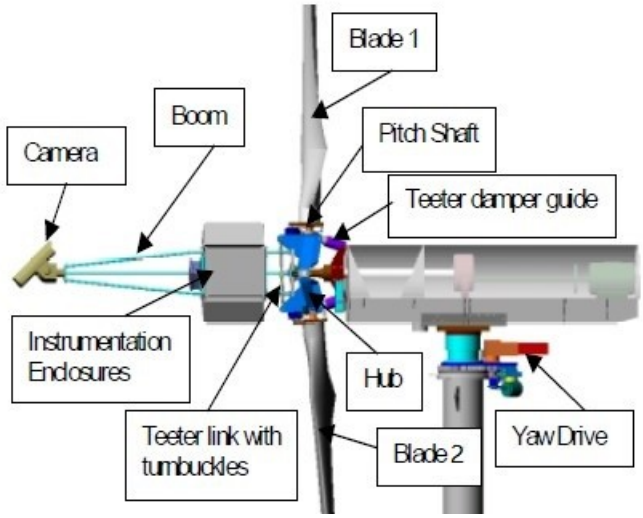

It is possible that the instrumentation enclosures have affected the flow field near the hub, which explains the discordance between the simulation results and experimental data at that position. From various CFD studies, the accuracy of simulation results stop changing too much after the number of mesh elements exceeds 15 million. Nonetheless, finer meshes around the blade surface give more accurate results up to certain points. The power output is lower than the experimental data by 10 percent, which is common in similar CFD studies. For example, in Yen-Pin Chen's study **[41]**, the power output of the simulation is around 10 percent lower than the experiment. Similar results also occur in Potsdam's CFD study on the aerodynamic behavior of the NREL phase VI rotor **[42]** and numerical research conducted by S.Derakhshan and A.Tavaziani **[43]**. Both of the studies gained good accuracy from pressure distribution on blade surface but the power outputs are almost 10 percent lower than the experimental data. This issue is not only limited to CFD simulations with unstructured mesh. In a collaborative research by Mukesh and Eswara Rao **[44]**, the CFD simulation has a structured mesh with good quality, but the simulation result of power output under 10m/s wind speed is almost 20 percent lower than experimental data even though the results of thrust is considerably accurate, which indicates that there is limitation of current CFD study in 3D rotational flow fields. CFD method provides an excellent approach to study aerodynamic characteristics as well as to observe flow fields around the HAWT blade and wind turbine wakes. However, various studies show that the accuracy of CFD simulation depends largely on the turbulence model selection and there is not a global approach that is suitable for all conditions, which means the turbulence model and control settings should be carefully chosen for every simulation **[45]**. Aiming to obtain accurate unsteady CFD simulation, two preconditioned transient CFD methods

for analysis of wind turbine flows have been developed by Sergio's research team **[46]**. One of which is a structured explicit Euler solver and the other one is an unstructured implicit Euler/RANS solver developed for wind turbine CFD.

4.3 Optimization Method: Goal Driven Optimization(GDO)

In the optimization process, a direct optimization tool in ANSYS WORKBENCH has been adopted. The direct optimization tool is based on the Goal Driven Optimization method where the objective is the output parameter which has to be optimized (maximized or minimized), while the input parameters are the design point domain.

In order to conduct optimization, a relatively accurate simulation should be complete. However, a simulation using a coarse mesh setup could be used to obtain a quick solution which will be used to narrow down the domain, the optimum region, where the global optimum lies. And the optimum region will be used as the boundary in the next optimization where a fine mesh is used to achieve high accuracy, which will significantly reduce the time cost. It is the high performance computing (HPC) that makes the optimization method feasible.

Figure 27: Simplified foil shape and design parameter

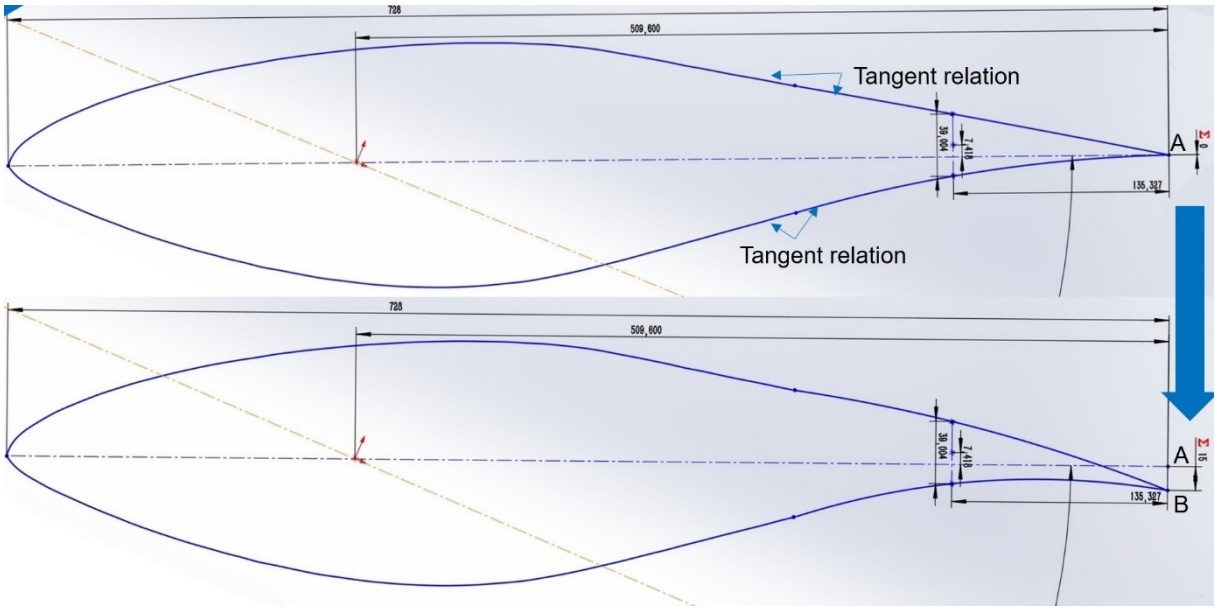

The blade model consists of 20 sections, in each section, the perpendicular distance from the new trailing edge position to the original position is set as the input parameter. Starting from the left to the right or from root to the tip are Section 1 to Section 20.

Figure 28: blade model

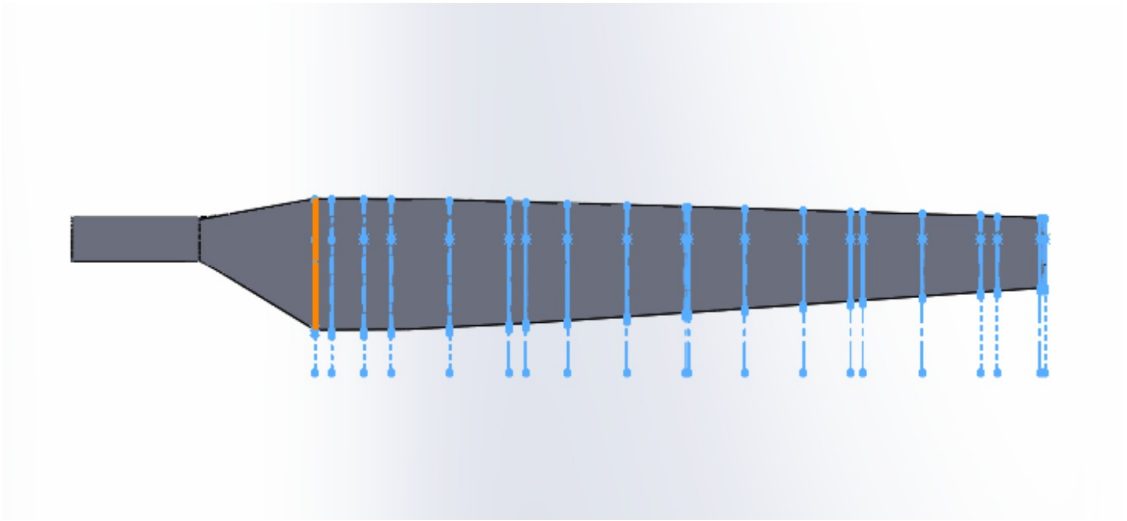

There are 6 different methods in goal driven optimization: Screening (Shifted Hammersley), MOGA (Multi-objective Genetic Algorithm), NLPQL(Non-linear Programming by Quadratic Lagrangian), MISQP(Mixed-Integer Sequential Quadratic Programming Method for Direct Optimization and Response Surface Optimization Systems), Adaptive Single-Objective Method for Direct Optimization systems, Adaptive Multiple-Objective Method for Direct Optimization systems. In this study, NLPQL(Non-linear Programming by Quadratic Lagrangian) and MISQP(Mixed-Integer Sequential Quadratic Programming) Method are selected for fast optimization and final optimization respectively.

Figure 29: Direct Optimization Structure

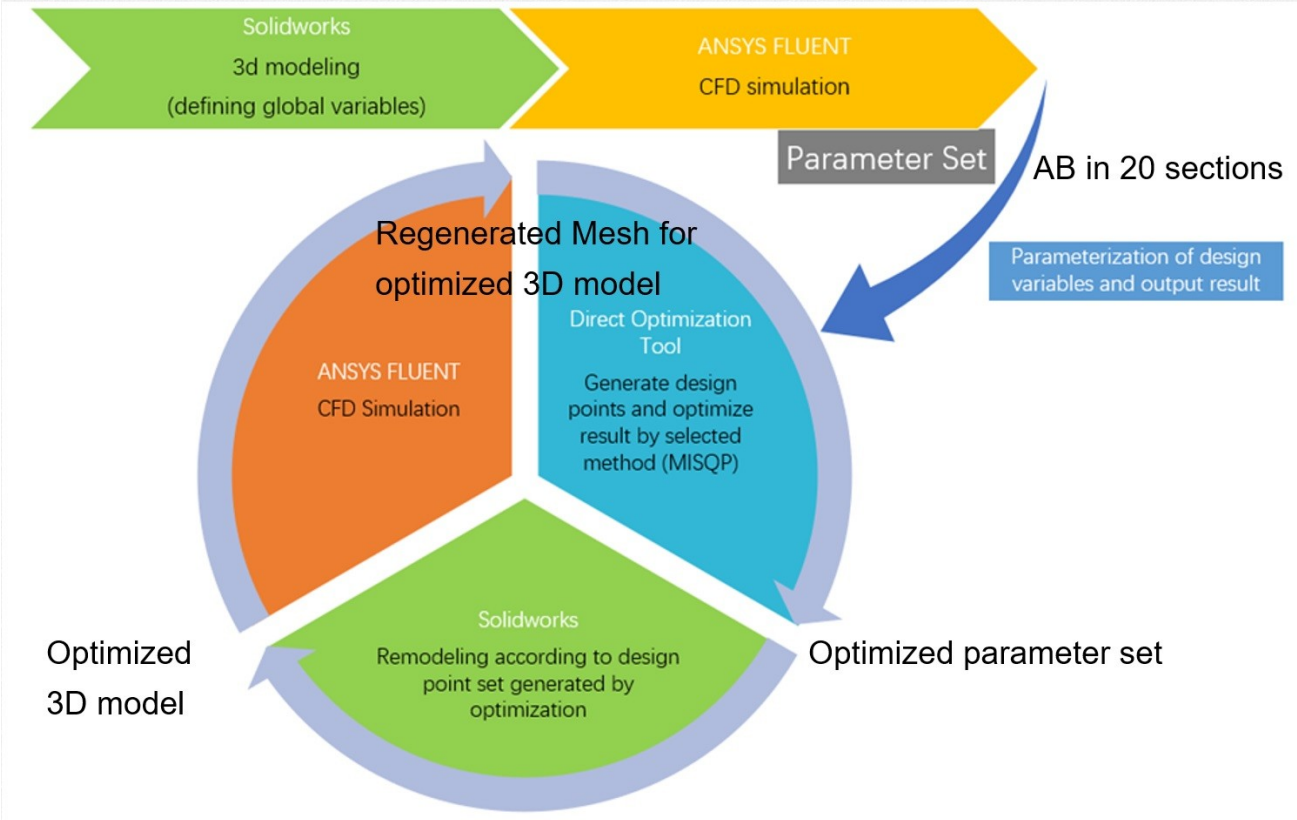

NLPQL(Non-linear Programming by Quadratic Lagrangian) method is a gradient-based single objective optimizer which is developed by Klaus Schittkowski on the basis of quasi-Newton methods. By quasi-Newton method, a problem of searching for an extrema of a scalar-valued function can be solved by searching for the zero of the gradient of that function instead of finding the minimum or the maximum of the function value, which means that the Jacobian of the gradient is equal to the Hessian of the original function that needs to be optimized. Moreover, the key property of this method which is most valued and exploited is that the Hessian matrix is a symmetric matrix, unlike Jacobian in finding the zeros of the gradient of the original function. One of the assumptions of this method is that both the objective function and constraints are continuously differentiable. To solve the problem, the idea behind this method is to generate a sequence of quadratic programming subproblems obtained by a quadratic approximation of the Lagrangian function and linearization of the constraints.

Figure 30:NLPQL optimization process

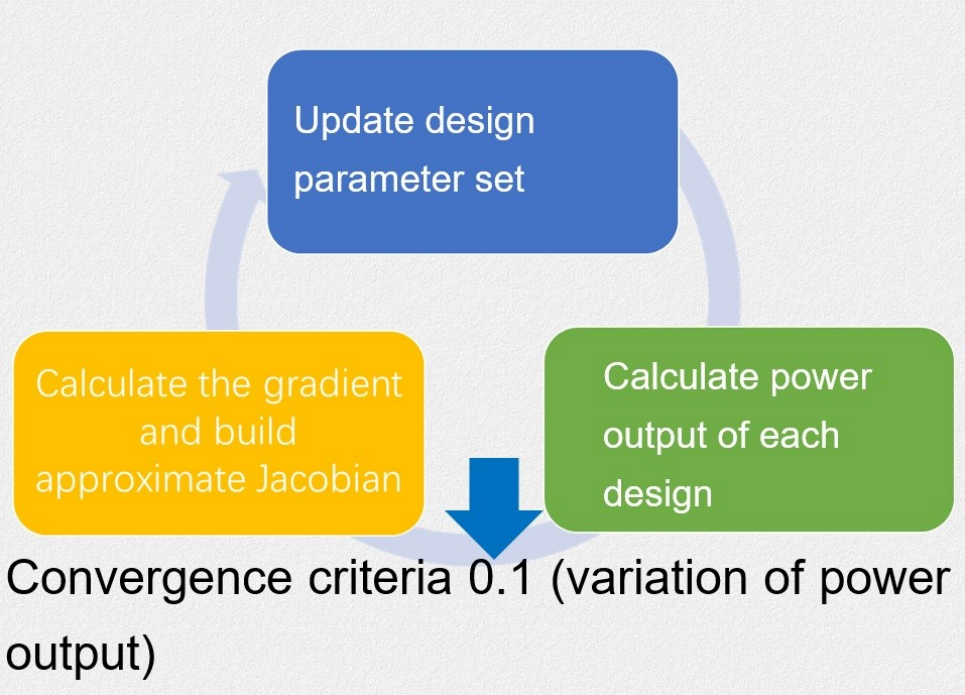

Table 1: Input design parameter set

position	parameter value(mm)
Section1	0-35 continuous
Section2	0-35 continuous
Section3	0-35 continuous
Section4	0-35 continuous
Section5	0-35 continuous
Section6	0-35 continuous
Section7	0-35 continuous
Section8	0-35 continuous
Section9	0-35 continuous
Section10	0-35 continuous
Section11	0-35 continuous
Section12	0-35 continuous
Section13	0-35 continuous
Section14	0-35 continuous
Section15	0-35 continuous
Section16	0-35 continuous
Section17	0-35 continuous
Section18	0-35 continuous
Section19	0-35 continuous
Section20	0-35 continuous

Table 2: Output: ranges of optimized design parameter set

position	parameter

	value(mm)
Section1	15 ~25
Section2	15 ~25
Section3	15 ~25
Section4	15 ~25
Section5	15 ~25
Section6	15 ~25
Section7	15 ~25
Section8	15 ~25
Section9	15 ~25
Section10	15 ~25
Section11	15 ~25
Section12	15 ~25
Section13	15 ~25
Section14	10~20
Section15	10~20
Section16	10~20
Section17	10~20
Section18	5~15
Section19	5~15
Section20	5~15

Though this method is considered the fastest among all the methods available in the toolbox, it can only handle continuous input parameters which makes it suitable for the first raw optimization process which is only aimed to narrow down the region where lies the optimum solution.

Since continuous input parameter set leads to redundant design point sets which make the optimization process considerably time-consuming, it is best to define discrete input parameter set which contains only a few values. And based on the first raw optimization, the optimum region is narrowed down and the new discrete optimization input parameters sets are shown in Table 3 below.

Table 3: Discrete input parameters in parameter set

position	discrete parameter set (mm)		
sec1	15	20	25
sec2	15	20	25
sec3	15	20	25
sec4	15	20	25
sec5	15	20	25
sec6	15	20	25
sec7	15	20	25
sec8	15	20	25
sec9	15	20	25
sec10	15	20	25
sec11	15	20	25
sec12	15	20	25
sec13	15	20	25
sec14	10	15	20
sec15	10	15	20
sec16	10	15	20
sec17	10	15	20
sec18	5	10	15
sec19	5	10	15
sec20	5	10	15

After the raw optimization, the final optimization using fine mesh and discrete input parameters is conducted. The final optimization uses MISQP(Mixed-Integer Sequential Quadratic Programming) Method and relies heavily on high performance computing. However, this method is much faster than other methods that can process discrete input parameters.

MISQP(Mixed-Integer Sequential Quadratic Programming) Method is a method that solves single objective optimization problems by modified sequential quadratic programming method and is available for both discrete and continuous input parameters **[47]**. This method is often used to solve mixed-integer non-linear programming problems of the form:

$$\begin{aligned} &\min \quad f_0(x) \\ &\text{s.t.} \quad f_i(x) \le 0, i \in I_1 := \{1,2,\ldots,m'\}, \qquad \text{problem(1)} \\ &\qquad f_i(x) = 0, i \in I_2 := \{m'+1, m'+2, \ldots, m\}, \end{aligned}$$

Where $f_i : R^n \to R (i \in \{0\} \cup I_1 \cup I_2)$ are the smooth functions. The feasible set and gradients of problem(1) are as follows:

$$\Omega := \{x \in R^n : f_i(x) \le 0, i \in I_1; f_i(x) = 0, i \in I_2\},$$

and $g_i(x) := \nabla f_i(x), i \in \{0\} \cup I_1 \cup I_2$.

Sequential quadratic programming(SQP) algorithm is widely used and proved highly effective in solving problem(1). SQP generates iteratively the main search directions by solving the standard quadratic programming subproblem as:

$$\begin{aligned} &\min \quad g_0(x)^T d + \frac{1}{2} d^T H d \\ &\text{s.t.} \quad f_i(x) + g_i(x)^T d \le 0, i \in I_1; f_i(x) + g_i(x)^T d = 0, i \in I_2 \end{aligned}$$

where $H \in R^{n \times n}$ is denoted as a symmetric definite matrix. Then a line search is performed to determine a step length, and to obtain the next iteration point.

However, in the subproblem, the equality constraints are hard to be satisfied so the SQP algorithm may fail to solve the problem. And to overcome this

difficulty, a new approach is proposed by Mayne and Polak **[48]**. The original problem is transformed into problem (2) as

$$\min \quad F_c(x) := f_0(x) - c\sum_{i \in I_2} f_i(x) \qquad \text{problem (2)}$$

$$\text{s.t.} \quad f_i(x) \le 0, i \in I,$$

where $I := I_1 \cup I_2$ and parameter $c > 0$.

feasible set $\Omega := \{x \in R^n : f_i(x) \le 0, i \in I\}$.

In addition, several further applications and advantages can be seen in **[49,50,51]**.

After linearization of all constraints and establishment of a quadratic approximation of the Lagrangian function, mixed-integer quadratic programs are successively generated and solved. To stabilize the algorithm, a trust region method is introduced to the process. However, when the optimization problem does not involve any constraints, Newton's method is used instead.

Figure 31:MISQP optimization process

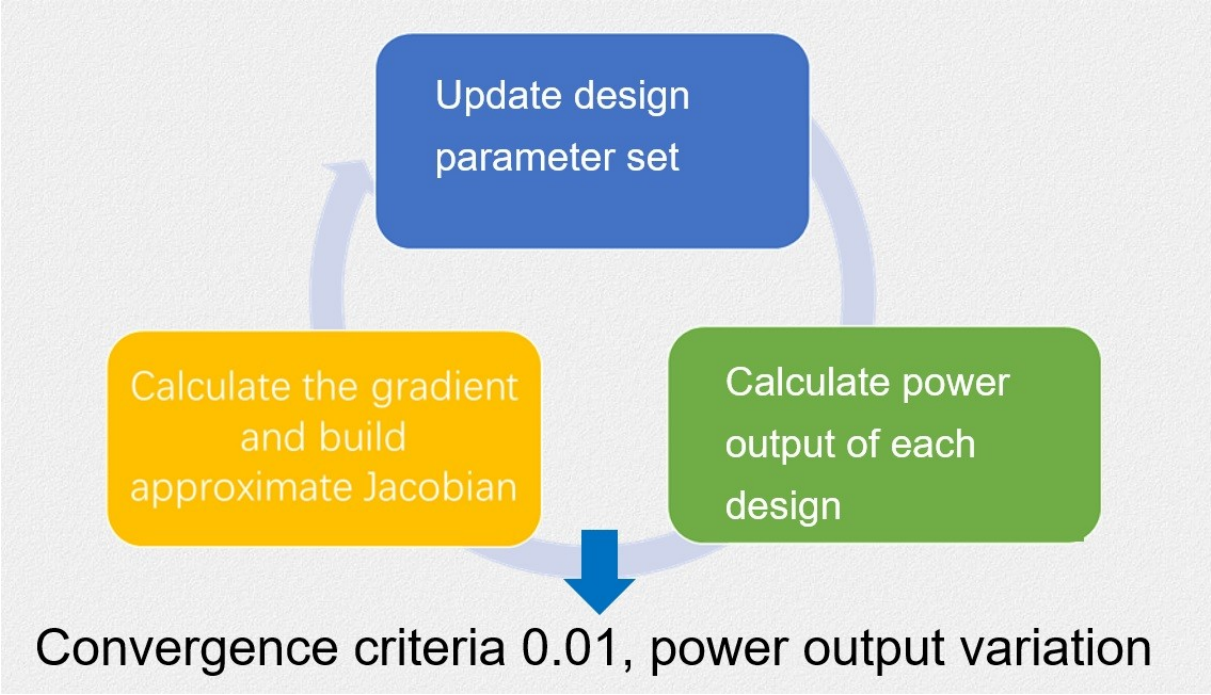

Before the final optimization, individual transient CFD simulations have been carried out in order to verify the accuracy of the raw optimization. In this case, three blade models have been built and their parameters are shown below in Table 4.

Table 4: Geometric parameters of the 3 blade models

	parameter values (mm)		
design parameter	Model 1	Model 2	Model 3
parameter1	15	20	25
parameter2	15	20	25
parameter3	15	20	25
parameter4	15	20	25
parameter5	15	20	25
parameter6	15	20	25
parameter7	15	20	25
parameter8	15	20	25
parameter9	15	20	25
parameter10	15	20	25
parameter11	15	20	25
parameter12	15	20	25
parameter13	15	20	25
parameter14	10	15	20
parameter15	10	15	20
parameter16	10	15	20
parameter17	10	15	20
parameter18	5	10	15
parameter19	5	10	15
parameter20	5	10	15

The simulation results are then compared with the original design to verify the accuracy of the raw optimization.

Table 5: CFD simulation results of 3 models

models	power output (W)	improvement
original model	8799.24	0
model 1	9447	7.40%
model 2	9589.18	8.97%
model 3	9412.25	6.97%

Simulation results show improvements in all three modified models and model 2 is the best so far, which proves that the row optimization process is accurate and the final optimization process can be conducted.

5.Final Optimization Results

Table 6:Computation requirements

Total CPU time	126h
Number of processors	16 cores
Number of mesh elements	19.8 million

Table 7:Optimal design points and power output

position	parameter value(mm)
Section1	15
Section2	15
Section3	15
Section4	15
Section5	15
Section6	15
Section7	15
Section8	15
Section9	15
Section10	15
Section11	15
Section12	15
Section13	20
Section14	10
Section15	10
Section16	10
Section17	10
Section18	5
Section19	5
Section20	5

Table 8: Comparison with the original model

Models	Power Output(W)	Improvement
Original Model	8799.24	
Final Design	9605.65	9.16%

As shown in Tables 6, 7 and 8 above, the final solution obtained from the optimization has a power output of 9605.65 W with an increase by 9.16%, compared to the original model, proving that the optimization is successful.

Figure 32:Pressure contour at 47 percent span

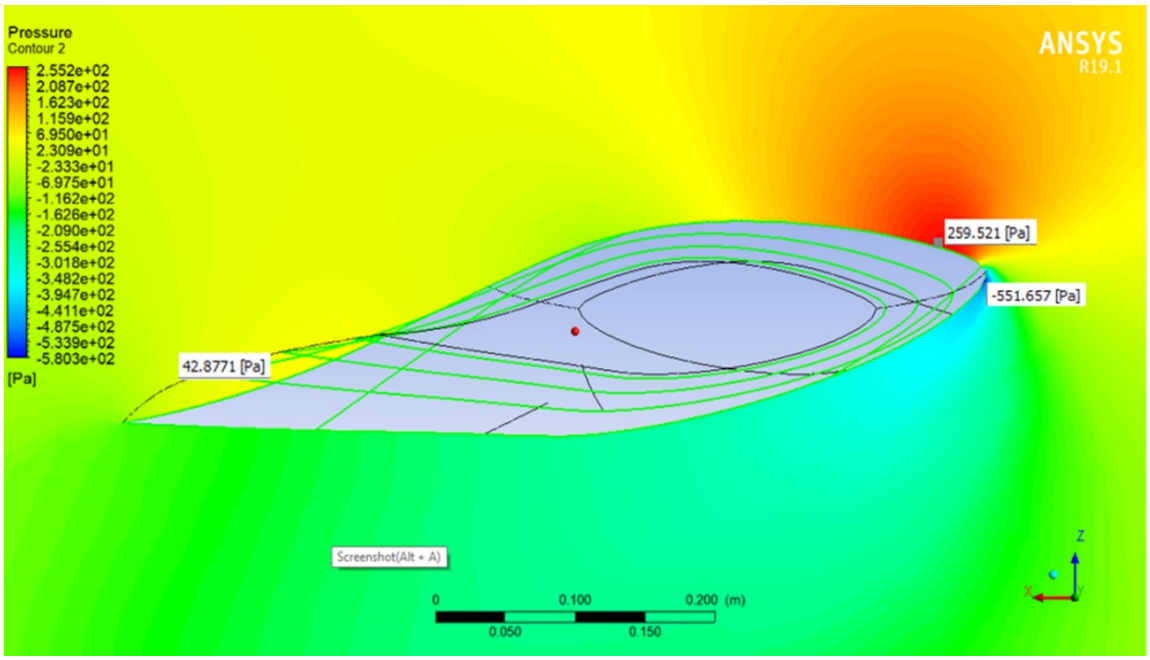

Original model

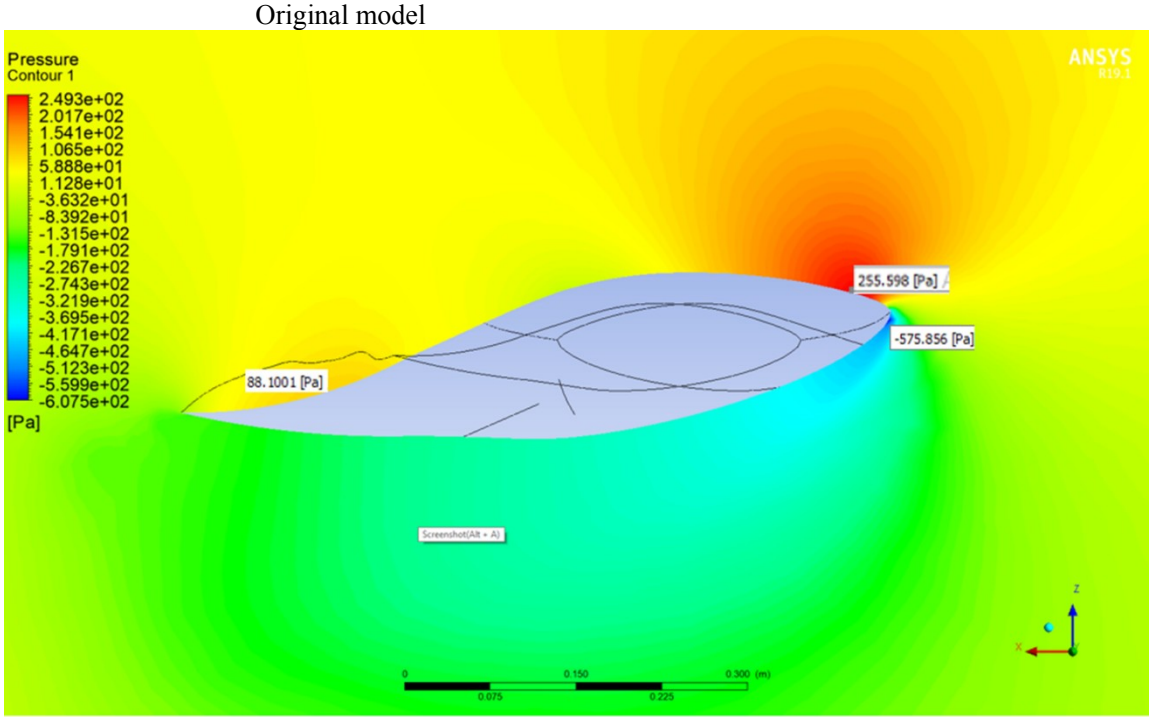

Modified model

As shown in Figure 32, near the trailing edge, the modified model has a pressure near the trailing edge on the pressure surface twice as much as the pressure in the original model. And the pressure distribution only changed slightly in the leading edge.

Figure 33:Pressure contour at 63 percent span

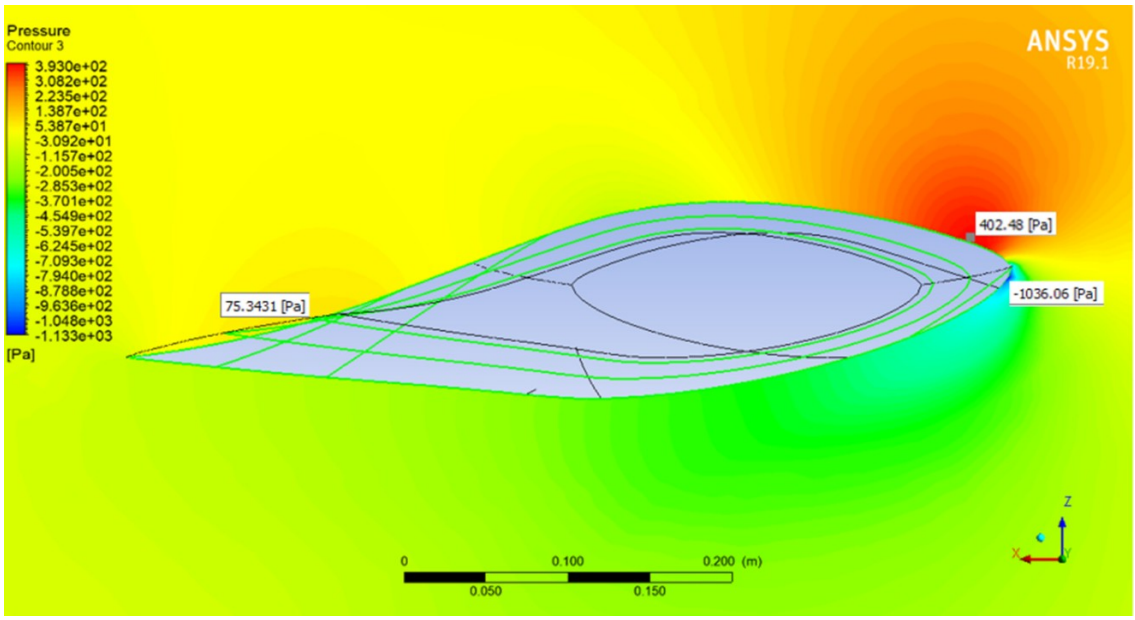

Original model

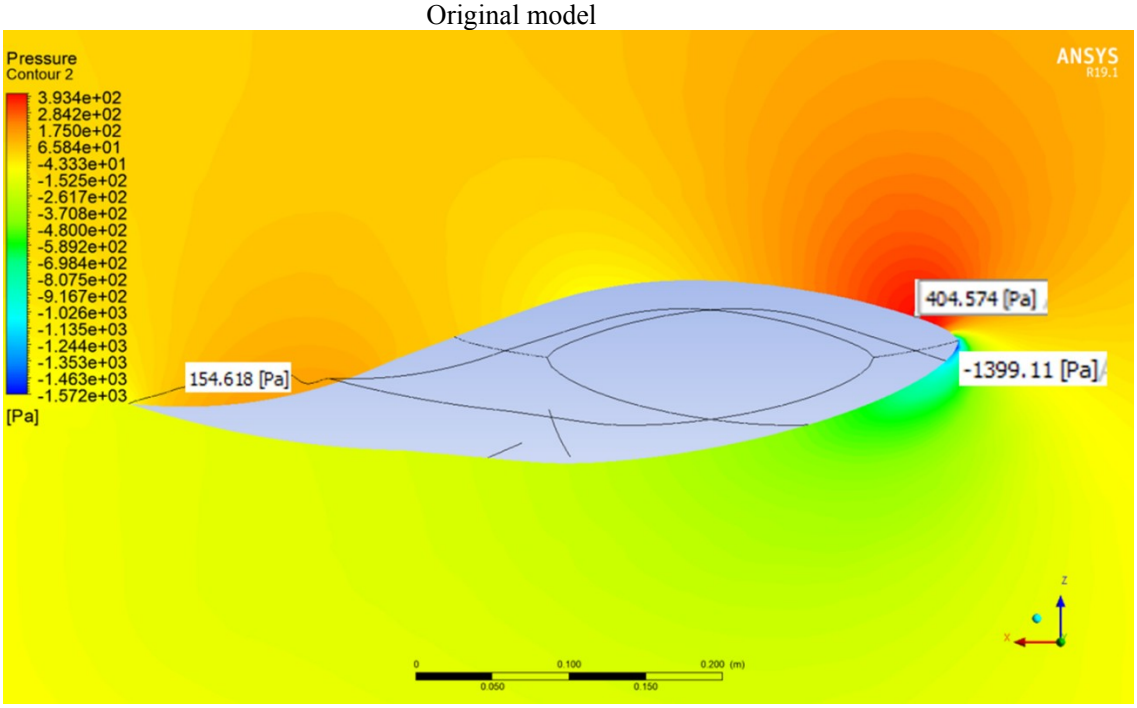

Modified model

And at the 63 percent span cross-section in Figure 33, similar results are found where the pressure value on the pressure surface near the trailing edge is more than double that of the original design. At the same time, the pressure distribution almost remains the same near the leading edge.

Figure 34:Pressure contour at 80 percent span

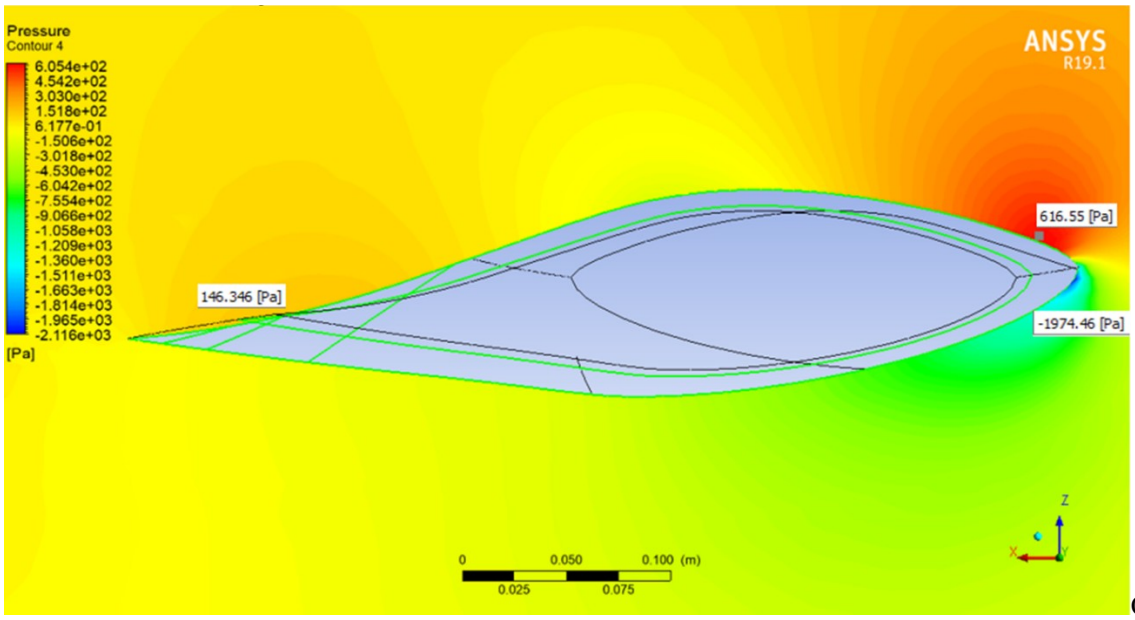

Original model

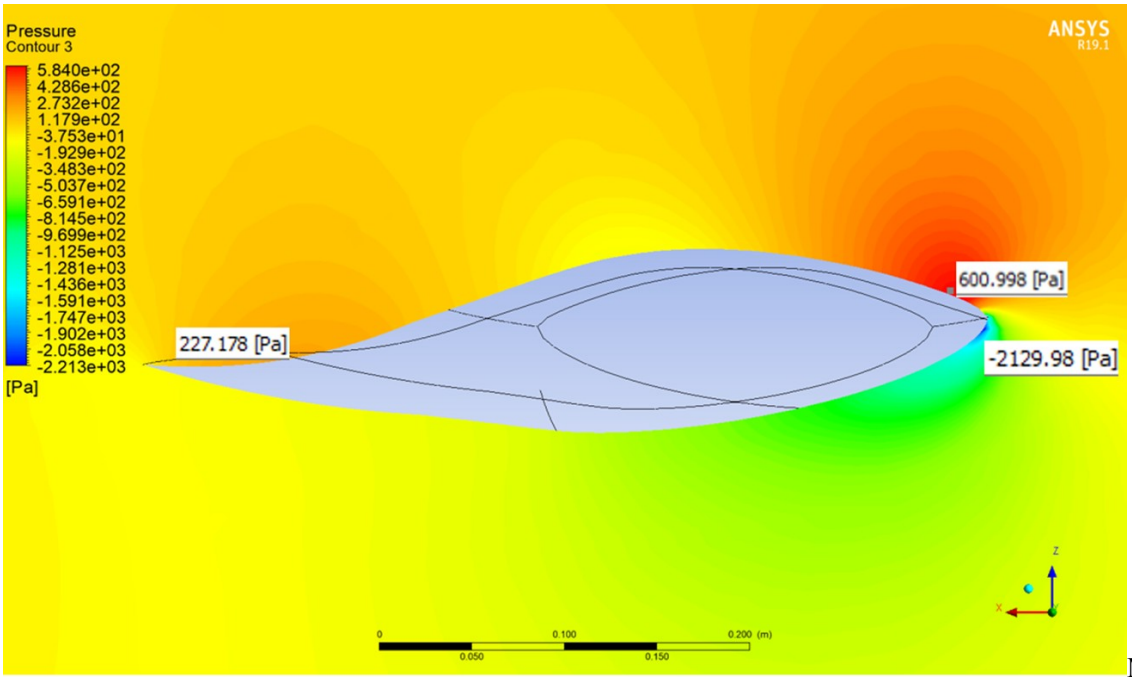

Modified model

At 80 percent span as shown in Figure 34, the pressure increases from around 146 Pa to 227 Pa near the trailing edge on the pressure side of the blade. On the contrary, the pressure distribution near the leading edge only changes slightly.

Figure 35:Pressure contour at 95 percent span

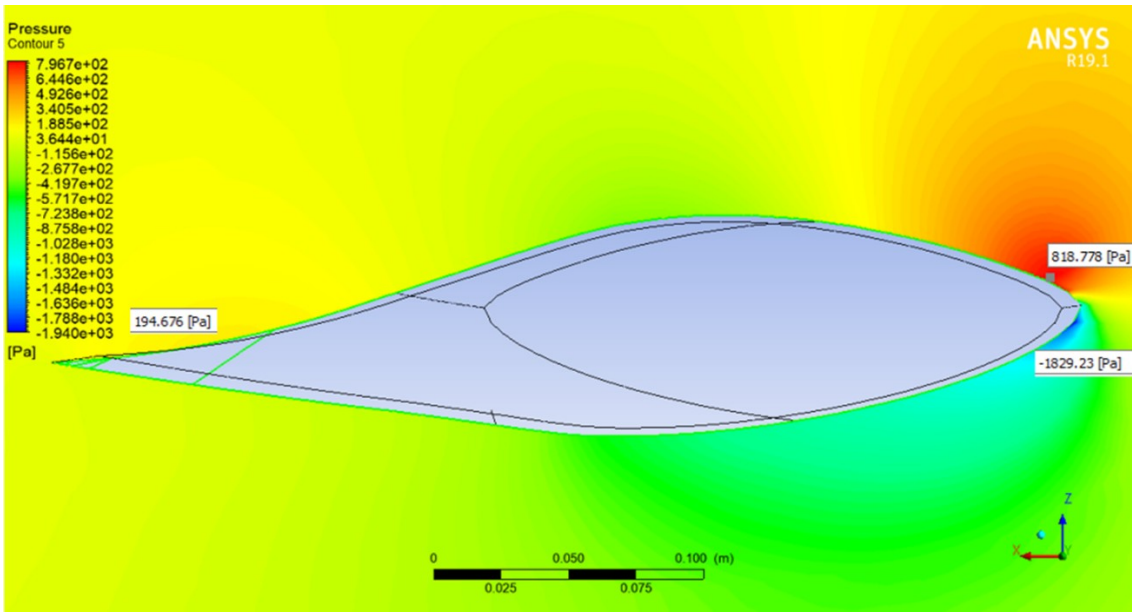

Original model

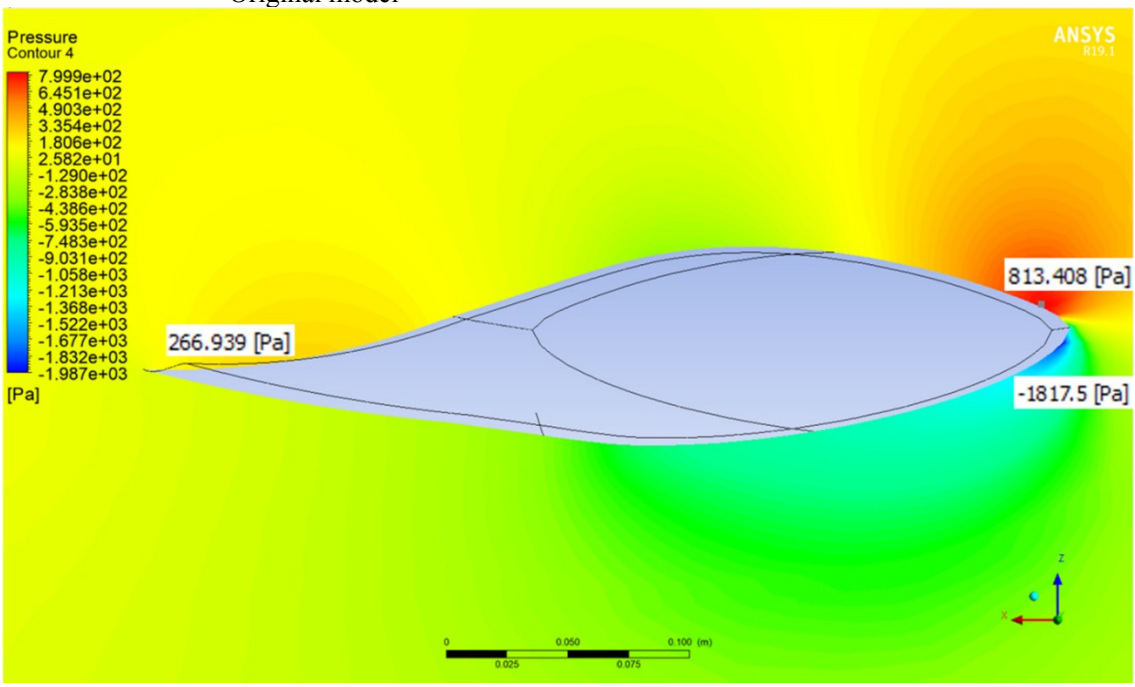

Modified model

And near the tip as 95 percent span, as seen in Figure 35, the pressure on the pressure surface near the trailing edge rises from around 195 Pa in the original design to 267 Pa in the optimized one, whilst the pressure distribution near the leading edge still remains almost the same. Inclusion, the optimized design increases the power output by increasing the pressure on the pressure surface of the blade near the trailing edge by using the optimal trail edge position.

6.Conclusion:

This study has successfully conducted a fully autonomous optimization process for the NREL Phase VI wind turbine blade using the built-in optimization toolbox in Ansys after the transient CFD simulation of the turbine has been validated. A 9% increase in power output is achieved, which makes the new model more efficient than the original one. If this is applied in the industry it will significantly lower the cost of wind power. Furthermore, the simulation itself shows good accuracy, which proves that the boundary conditions and turbulence model chosen in this study are the right choices. Nevertheless, further improvement can be achieved by tuning different control settings and combine them with other near wall treatment functions. Most importantly, it proves that the design approach of changing the airfoil shape with optimal flap angle will indeed increase lift.

Results show a significant increase in the pressure near the trailing edge, which is caused by the increased flap angle near the trailing edge of the new model. When airflow passes the remodeled area, the pressure on the pressure side of the blade near the trail edge increases, resulting in higher lift and thus greater power output. In the future work, a longer 3D URANS simulation with smaller time step size will be conducted in order to observe the fluctuation in the power output, and the results will be compared to steady-state simulation to study the difference.

Thanks to the powerful and user-friendly optimization toolbox, a multi-objective optimization can be performed in the future. Instead of only aiming to increase the power output without any constraint, mass and/ or the structural strength can be taken into consideration in the future optimization. For example, the power output will be maximized without causing too much increase in the mass that makes cost rise. Even a more sophisticated model that consists of multiple design variables can be optimized using this method, which makes the design process more efficient and less expensive. Furthermore, if sufficient engineering data is available, combining this method with neural-network optimization algorithm, the framework can design the wind turbine blades with the best aerodynamic performance under certain conditions, such as fluid-structure interaction.

Reference

1. IEA global energy report
2. 张维志，李方洲，小型水平轴风电机风洞试验---Weizhi Zhang, Fangzhou Li, Small wind turbine wind tunnel experiment.
3. Wind Energy Handbook, Tony Burton,David Sharpe,Nick Jenkins,Ervin Bossanyi
4. 倪受元， 风力发电机设计----Shouyuan Ni, Wind turbine design
5. Global wind report
6. KAZENERGY Report
7. Wind power potential in Kazakhstan, Atlas
8. Wind energy handbook, Tony Burton,David Sharpe,Nick Jenkins,Ervin Bossanyi
9. Windworks.org by Paul Gipe
10. Vertical Axis wind turbines: Great in 1890, Also-rans In 2014, Michael Barnard
11. Vertical axis wind turbines, Richard Smith
12. What are vertical axis wind turbines? By Eric Eggleson
13. Exploit Nature—Renewable Energy technologies by Gurmit Singh
14. 蒋超奇，严强， 水平轴与垂直轴风力发电机的比较---Chaoqi Jiang, Qiang Yan, comparison of HAWT and VAWT
15. Innovation in wind turbine design by Peter Jamieson
16. GE renewable energy
17. Modular wind energy device by Brill Bruce
18. Navid Goudarzi; Weidong Zhu (November 2012). "A Review of the Development of Wind Turbine Generators Across the World”
19. John Gardner, Nathaniel Haro & Todd Haynes (October 2011). "Active Drivetrain Control to Improve Energy Capture of Wind Turbines"
20. Vertical-Axis Wind Turbines by Richard Smith
21. Aero-structural Design Optimization of Composite Wind Turbine Blade. Naishadh G, Vasjaliya, Sathya N.Gangadharan; Embry-Riddle Aeronautical University
22. Aerodynamic shape optimization of wind turbine blades using a Reynolds-averaged Navier-Stokes model and an adjoint method. Tristan Dhert, Turaj Ashuri, Joaquim R.R.A.Martins
23. Aerodynamic Shape Optimization of Wind Turbine Blades Using a Parallel Genetic Algorithm. Ozge Polat, Ismal H.Tuncer, Parallel Computational Fluid Dynamics Conference, 2013
24. Horizontal axis wind turbine rotor blade: winglet and twist aerodynamic design and optimization using CFD. Monier Ali Elfarra, Middle East Technical University
25. Momentum theory,Wikipedia
26. Manwell, J. F.; McGowan, J. G.; Rogers, A. L. (February 2012). Wind Energy Explained: Theory, Design and Application. Chichester, West Sussex, UK: John Wiley & Sons Ltd. pp. 92–96. ISBN 9780470015001.
27. Enercon E-family, 330 Kw to 7.5 Mw, Wind Turbine Specification
28. Wind Turbine Blade Analysis using the Blade Element Momentum Method. Version 1.1 Grant Ingram
29. An extension of BEM method applied to horizontal-axis wind turbine design Jerson Rogério Pinheiro Vaz, João Tavares Pinho, André Luiz Amarante Mesquita
30. Sant T, Improving BEM-based aerodynamic models in wind turbine design codes. Department of Mechanical Engineering, University of Malta; 2007.
31. Macquart T, Maheri A, Busawon K. Improvement of the accuracy of the blade element momentum theory method in wind turbine aerodynamics analysis. Proceedings of the 2nd international symposium on environment-friendly energies and applications (EFEA); 2012

32. PJ M, AC H. Aerodynamic theory manual. National Renewable Energy Laboratory; 2005
33. DM P, DA P. Theoretical prediction of dynamic-inflow derivatives. Vertica 1981; 5:21-34
34.H G. A general theory of the autogiro. Report and Memorandum No.1111. UK: British ARC; 1926
35. de Vries O. Fluid dynamic aspects of wind energy conversion. VA: DTIC; 1979.
36. Snel H, Houwink R, Bosschers J. Sectional prediction of lift coefficient on rotating wind turbine blades in stall. Netherlands Energy Research Foundation, Petten; 1994
37. ML B. A new empirical relationship between thrust coefficient and induction factor for the turbulent windmill state. Netherlands Renewable Energy Laboratory; 2005
38.3D MULTIDISCIPLINARY AUTOMATED DESIGN OPTIMIZATION TOOLBOX FOR WIND TURBINE BLADES Sagi Sagimbayev, Yong Zhao , S.C. Fok, Soo Lee Teh
39.H.K. and Malalasekera,W.Versteeg, An introduction to computational fluid dynamics-The finite volume method. Essex, England: Longman Scientific & Technical, 1995.
40.NTNU, Lecture notes in TEP4112 Turbulent Flows. Trondheim: NTNU, 2010.
41.A study of the aerodynamic behavior of a NREL phase VI turbine using the CFD methodology. Yen-Pin Chen, Wright State University.
42.Unstructured mesh CFD aerodynamic analysis of the NREL phase VI rotor. Mark A. Potsdam, Aeroflightdynamics Directorate(AMRDEC), U.S.Army Research, Development and Engineering Command, University of Wyoming Wind Energy Research Center, Moffett Field, CA 94035. Dimitri J.Mavriplis, Wind Energy Research Center, University of Wyoming, Laramie, WY 82071.
43.Study of Wind Turbine Aerodynamic Performance Using Numerical Methods. S.Derakhshan and A.Tavaziani
44.CFD prediction of NREL Phase VI Rotor Experiments in NASA/AMES Wind tunnel. Mukesh M.Yelmule, EswaraRao Anjuri VSJ, International Journal of Renewable Energy Research, Vol3, No.2, 2013.
45.Chi-Jeng Bai, Wei-Cheng Wang. Review of computational and experimental approaches to analysis of aerodynamic performance in horizontal-axis wind turbines(HAWTs).
46.Development of Efficient and Accurate CFD Technologies for Wind Turbine Unsteady Aerodynamics. M.Sergio Campobasso, Aldo Bonfiglioli, Mohammad Baba-Ahmadi; The 14th international Conference on Fluid Flow Technologies; Budapest, Hungary; September 9-12, 2009.
47. An improved sequential quadratic programming algorithm for solving general nonlinear programming problems. Chuan-Hao Guo, Yan-Qin Bai, Jin-Bao Jian; Journal of Mathematical Analysis and Applications, Appl,409(2014)777-789
48. D.Mayne, E.Polak. Feasible direction algorithm for optimization problems with equality and inequality constraints. Math. Program.11(1976)67-80.
49. J.Herskovits. A two-stage feasible direction algorithm for nonlinear constrained optimization. Math. Program. 36(1986) 19-38.
50. J.Jian, C.Guo, L.Yang. A new generalized projection method of strongly sub-feasible directions for general constrained optimization. Pac.J.Optim. 5(2009)507-523.
51. C.Lawrence, A. Tits; Nonlinear equality constraints in feasible sequential quadratic programming. Optim. Methods Softw. 6 (1996) 252-282.
52. S. Patankar. Numerical Heat Transfer and Fluid Flow, CRC Press (1980).